

Diler Katircioğlu-Bayel

Original Research

Using Glycerin, a By-Product of Biodiesel, as a Grinding Aid in the Dry Grinding of Marble Dust Waste

Sorokhaibam Khaba

Original Research

Analysis of Bottleneck using Mine Production Index and Ishikawa Diagram: A Case of Indian Coal Mine

Jinyi Ji
Baokun Zhou
Zhichen Tao
Xiaoqing Chen

Original Research

Multi-Factor Optimization of Adjacent Layered Salt Rock Storage Based on Response Surface Methodology

Jiaqi Wang

Original Research

Study on Floor Instability Law of Cemented Filling Mining above a Confined Aquifer

Firat Atalay

Original Research

Comparison of Conditioned Radial Basis Function Approach and Kriging: Estimation of Calorific Value in a Coal Field



Scientific Mining Journal

Vol: 62, No: 2, June, 2023

A peer-reviewed quarterly journal of the Chamber of Mining Engineers of Türkiye

Editor-in-Chief

Dr. A. Hakan Benzer, *Hacettepe University*

Editors

Dr. Hakan Dündar, *Hacettepe University*

Dr. Güneş Ertunç, *Hacettepe University*

Dr. Sedat Esen, *Esen Mining*

Dr. Murat Kademli, *Hacettepe University*

Dr. Mehmet Kızıl, *Queensland University*

Dr. Ece Kundak, *Eskişehir Osmangazi University*

Dr. Abdullah Obut, *Hacettepe University*

Dr. Ümit Özer, *Istanbul University - Cerrahpaşa*

Dr. Oktay Şahbaz, *Dumlupınar University*

Editor Assistants

Sena Naz Gökdemir

Melis Orakcı

AIMS AND SCOPE

Scientific Mining Journal, which is published in open access electronic environment and in printed, is a periodical scientific journal of Union of Chambers of Turkish Engineers and Architects Chamber of Mining Engineers. The name of the journal was "Mining" until June 2016 and it has been changed to "Scientific Mining Journal" since September 2016 because it can be confused with popular journals with similar names and the ISSN number has been updated from 0024-9416 to 2564-7024.

Scientific Mining Journal, published four times a year (March-June-September-December), aims to disseminate original scientific studies which are conducted according to the scientific norms and publication ethics at national and international scale, to scientists, mining engineers, the public; and thus to share scientific knowledge with society. The journal is in English.

The journal covers theoretical, experimental, and applied research articles, which reflects the findings and results of an original research in the field of mining engineering; review articles, which assess, evaluates, and interprets the findings of a comprehensive review of sufficient number of scientific articles and summarize them at present information and technology level; technical notes, which may be defined as a short article that describes a novel methodology or technique; a case studies, which are based on the theoretical or real professional practice and involves systematic data collection and analysis.

The journal gives priority to works that will enable the advancement of current available information necessary to serve humanity with nonrenewable mineral resources with the perspective of sustainable mining principles. In this context, mine exploration, mineral resource modeling, surveying, mine economics and feasibility, geostatistics, rock mechanics and geotechnics, diggability studies, underground and surface mining, mine design, support design in underground mines and tunnels, rock penetration and rock fragmentation, mine production planning and pit optimization, mine health and safety management, mine ventilation, methane emission and drainage in underground coal mines, mineral processing and beneficiation, process mineralogy, analytical techniques, mineral comminution, mineral classification and separation, flotation/flocculation, solid/liquid separation, physical enrichment methods, hydro and biometallurgy, production metallurgy, modeling and simulation, instrumentation and process control, recycling and waste processing, mining law, environmental health and management, transportation, machinery and equipment selection and planning, coal gasification, marble technology, industrial minerals, space mining, submarine mining and mechanization are included in the journal content.

Submitted manuscripts are evaluated by the editorial board and expert referees independently in accordance with the best practices in academic publishing. The publishing rights of the manuscripts, approved for publication at the end of the evaluation process, are transferred to the Chamber of Mining Engineers by the authors.

Scientific Mining Journal

Scientific Mining Journal is indexed or abstracted in:

SCOPUS

Google Scholar

ULAKBİM TR Dizin

GeoRef

OpenAIRE

*Author Instructions, Editorial Advisory Board, the Peer Review Process and Reviewer Lists
can be accessed from <http://www.mining.org.tr>*

Publication Ethics

*Complying with the research and publication ethics is considered an indisputable precondition to be
published. Publication Ethics can be accessed from <http://www.mining.org.tr>*

Scientific Mining Journal

Owner on behalf of the Chamber of Mining Engineers of Türkiye: Ayhan Yüksel

Responsible editing manager: Mehmet Erşat Akyazılı

Correspondence address:

Selânik Cad. No: 19/4 06650 Kızılay-Çankaya / Ankara Türkiye

Tel: +90 312 425 10 80 / +90 312 418 36 57 • Fax: +90 312 417 52 90

e-mail: smj@maden.org.tr

web: <http://www.mining.org.tr>

Publication type: Local periodical, quarterly

Design: Gülendem Gültekin

Printed at: Ziraat Gurup Matbaacılık Ambalaj San. ve Tic. A.Ş.

Printing date: 31.07.2023

CONTENTS

- | | | |
|---|----|--|
| Diler Katirciođlu-Bayel | 61 | <i>Original Research</i>
Using Glycerin, a By-Product of Biodiesel, as a Grinding Aid in the Dry Grinding of Marble Dust Waste |
| Sorokhaibam Khaba | 67 | <i>Original Research</i>
Analysis of Bottleneck using Mine Production Index and Ishikawa Diagram: A Case of Indian Coal Mine |
| Jinyi Ji
Baokun Zhou
Zhichen Tao
Xiaoqing Chen | 77 | <i>Original Research</i>
Multi-Factor Optimization of Adjacent Layered Salt Rock Storage Based on Response Surface Methodology |
| Jiaqi Wang | 85 | <i>Original Research</i>
Study on Floor Instability Law of Cemented Filling Mining above a Confined Aquifer |
| Firat Atalay | 93 | <i>Original Research</i>
Comparison of Conditioned Radial Basis Function Approach and Kriging: Estimation of Calorific Value in a Coal Field |





Original Research

Using Glycerin, a By-Product of Biodiesel, as a Grinding Aid in the Dry Grinding of Marble Dust Waste

Diler Katırcıoğlu-Bayel^{a,*}

^a Niğde Ömer Halisdemir University, Engineering Faculty, Mining Engineering Department, 51240 Niğde, TÜRKİYE

Received: 28 October 2022 • Accepted: 7 June 2023

A B S T R A C T

Glycerin represents the primary by-product of biodiesel generation when vegetable oil is transesterified with ethanol or methanol. It is essential to study how to prevent natural resource depletion and transform waste into usable and valuable products. Using glycerin as a grinding aid can be an alternative solution for utilizing the excess glycerin resulting from biodiesel production. This paper investigated the usability of unrefined glycerin as a grinding aid in the dry grinding of marble wastes in terms of grinding efficiency while planning to reduce the adverse impacts of waste on the environment via its efficient utilization. The dry grinding experiments conducted within the study's scope researched the impacts of five dosages (0%, 0.25%, 0.5%, 1%, and 2% by weight) on the product. The current research is promising in terms of preventing the depletion of natural resources and transforming waste into usable and valuable products. Furthermore, considerable enhancements were obtained in the grinding performance with the grinding aid utilized.

Keywords: Marble waste, Mineral filler, Dry grinding, Grinding aid, Recycling

Introduction

Like all industrial activities, the adverse influence of marble dust wastes (MDW) on the environment constitutes a problem, and waste management is also inevitable in natural stone plants. Moreover, industries have a social responsibility to protect the environment and ensure that natural resources are used sustainably. For a sustainable economy, environmental protection must accompany industrialization and utilizing natural resources (Mymrin, 1997). Nowadays, the need to turn to alternative materials is increasing daily due to developing technology, competition from industry, and the rapid consumption of the Earth's resources. The most crucial step in achieving the said balance is to ensure the reuse of the waste generated in one area within the same area, in another industrial sector, or for another aim, e.g., as a filler instead of calcite. MDW contains a high amount of calcium carbonate (El-Sherbiny et al., 2015). The excess CaCO₃ ratio in the chemical composition of MDW expands its usage area and provides the opportunity for its use instead of calcite, which is highly needed in the industry. Particle size is desired from

1-2 µm to 50-100 µm according to the sector used (DPT, 2001). Alyamac and Ince (2009) and Tunc (2018) reported the reuse of waste marble in the paper, plastic, chemical, glass, and fertilizer industries and construction activities. Nayak et al. (2022) assessed the physical and mechanical properties of MDW-filled polyester composites and reported that MDW was highly compatible as a potential filler in polyester resin up to 32% by weight. To use MDW as a filler instead of calcite, it must have a high degree of hydrophobicity and be able to be ground to ultrafine sizes. The prominent properties of composites are attributed to a small particle size, thus resulting in a large interface area and high surface energy of nanoparticle fillers, leading to strong interfacial adhesion between fillers and the polymeric matrix (Zhang et al., 2010). Bringing these wastes to the desired size is one of the most energy-consuming and costly processes. Improvements, albeit small, to be made at low costs in grinding processes consuming a lot of energy will provide significant economic benefits. Size reduction processes are highly affected by the physical and chemical conditions of the grinding medium. The inefficiency of

* Corresponding author: dkatircioglu@ohu.edu.tr • <https://orcid.org/0000-0002-0336-8770>

grinding, especially in dry grinding, is generally explained by the slowing effect caused by fine particles. This may originate from the regrowth or rebuilding of particles from smaller particles as a result of either agglomeration, including van der Waal's forces, or direct briquetting, or coating of balls for the purpose of providing soft surfaces (Austin et al., 1984; El-Shall and Somasundaran, 1984; Locher and Seebach, 1972; Orumwense and Forssberg, 1992). The use of chemical additives represents an economical alternative for industrial applications. The utilization of chemical additives does not influence the breakage of coarse material. However, it only becomes a factor when fine material is built up in the mill (Locher and Seebach, 1972). It is necessary to add chemicals under conditions that cause chemisorption on particles' surfaces and utilize a sufficient amount of additives with the objective of creating the adsorbed layer on the whole area of fine particles generated in the course of grinding. The impact of additives is reducing the van der Waal's adhesion force between fine particles, thus ensuring more effective breakage interactions between grinding media and particles through a mechanism that is not completely understood and reducing the formation of agglomerate in cases when this constitutes a problem. The adsorbed additive also provides improved powder flowability (Fuerstenau, 1995). Although grinding aids provide efficiency and reduce energy costs, they create a separate cost item since they are generally imported from abroad. In this context, as an alternative to these expensive, imported grinding chemicals, various waste/by-products are important in reducing costs and evaluating waste.

By-products and waste products can be grinding aids for effective size reduction and minimizing energy consumption. Using grinding aids, it is possible to increase the amount of production with the wanted product fineness, and a finer product can be obtained in an identical amount of production. There are many studies in the literature on the usability of various wastes and by-products as grinding aids. Gao et al. (2011) investigated whether utilizing beet molasses as a grinding aid for blended cement with high volumes of mineral admixtures was viable. Beet molasses (0.01–0.05% by weight of cement) was added at various ratios into a blended cement. Concerning the performance of the blended cement, beet molasses led to a higher compressive strength at 3 days and 28 days. Li et al. (2016) tried waste cooking oil (WCO) as a grinding aid while grinding cement clinker and gypsum. The findings demonstrated that WCO considerably enhanced cement grinding. In another study, Li et al. (2015) used recycled beet molasses as a grinding aid in cement generation. The results revealed in detail that the recycled beet molasses contributed to clinker grinding and improved other cement properties. Leoneti et al. (2012) investigated the utilization of glycerol, a by-product of biodiesel generation in Brazil. They stated that glycerol was used as one of the grinding chemicals, especially in the form of commercial mixtures. However, the mentioned glycerin has limited use because it is accepted as an unrefined raw material, which should be refined for its utilization in the future. Generally, 10 kg of glycerol is created as a by-product of each 100 kg of biodiesel generated (Chi et al., 2007). The study by Karinen and Krause (2006) showed that biodiesel generation produced almost 10% of glycerol by volume.

Reducing environmental problems from waste generation to its irresponsible disposal is based on the adequate

use of wastes in appropriate environments. Managing waste on a global scale is an essential and important strategy since it has become a critical factor for people, animals, and vegetation (Sabine, 2013). The nature, amount, and type of waste vary from country to country. Helping to preserve the quality of the environment and health requires looking for an effective way to manage waste appropriately. For these purposes, waste must be recycled, reused, and directed to a valuable and usable product. These days, the use of waste is a priority for sustainable development success. In this respect, it is necessary to investigate wastes produced in natural stone processing plants as mineral fillers in terms of both using these wastes and eliminating their negative environmental effects. The purposes of this paper are to investigate the effect of glycerin on the grinding efficiency of MDW. Experimental results were assessed based on several product properties like particle size distribution (d_{50}), size reduction (F_{90}/P_{90}), grinding media coating, and energy consumption. This study is important since, to the best of our knowledge, it is the first study in the literature that compares the usability of by-products as grinding aids on the waste calcitic and dolomitic marble in mineral filler production.

1. Materials and methods

1.1. Materials

There are two subclasses of marble, calcitic (CaCO_3) and dolomitic ($\text{CaMg}(\text{CO}_3)_2$). The current research utilized Afyon white (calcitic) marble and Aydın yellow (dolomitic) marble wastes (Figure 1). After drying waste samples in an oven at a temperature of 60 °C to a constant weight, the feed size (< 2 mm) required for the conventional ball mill was produced, which was crushed in two stages with a jaw and hammer crusher. Canada Acme Lab analyzed the chemical properties of the marble wastes utilized in the above-mentioned tests by employing the ICP-MS method. Table 1 presents the materials' chemical content.

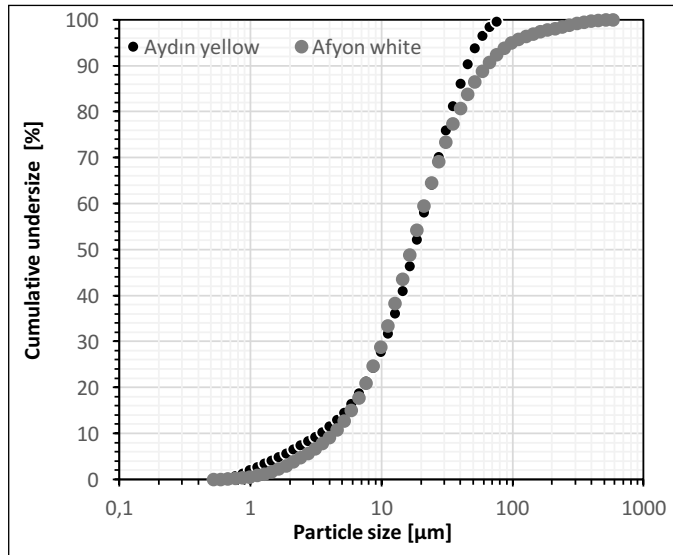


Figure 1. The appearance of Afyon white (calcitic) marble and Aydın yellow (dolomitic) marble dust

Table 1. ICP-MS elemental analysis of the calcitic and dolomitic marble wastes (in wt%)

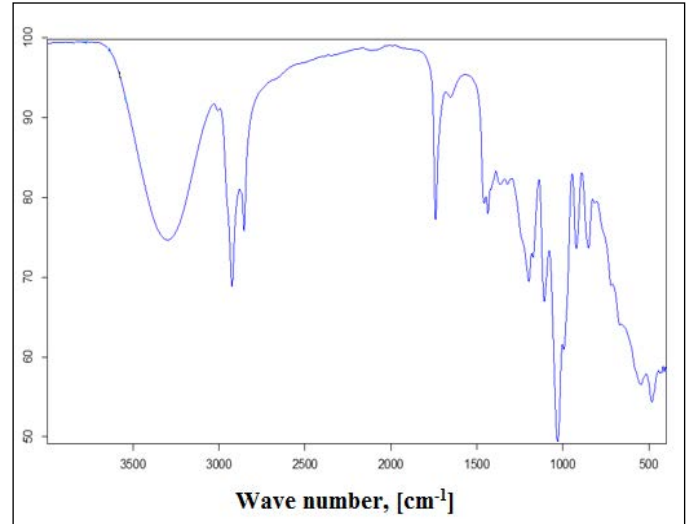
Sample	CaO	MgO	SiO ₂	Al ₂ O ₃	Fe ₂ O ₃	MnO	Na ₂ O	K ₂ O	Cr ₂ O ₃
Afyon white	55.86	0.36	0.29	0.05	<0.04	<0.01	0.02	0.02	<0.002
Aydın yellow	30.56	21.21	0.09	0.03	0.24	0.01	0.01	<0.01	<0.002

Test samples with an average particle size of $d_{50}=16.9 \mu\text{m}$ for calcitic marble and $d_{50}=17.8 \mu\text{m}$ for dolomitic marble were used in grinding studies (Figure 2). The unit weights of calcitic marble powder ($\gamma_s = 2.68 \text{ g/cm}^3$) and dolomitic marble powder ($\gamma_s = 2.78 \text{ g/cm}^3$) were determined with a pycnometer (ASTM D 854-02). High-density (6000 kg/m^3) yttria-stabilized zirconia (ZrO₂) grinding media purchased from Cenotec Co., Ltd., Korea, were used in the ultrafine grinding experiments.

**Figure 2.** Particle size analysis of the samples used in the experiments

Unrefined glycerin, a light yellow transparent liquid, is obtained while producing biodiesel. Glycerin was provided by the Kolza Biodizel Fuel and Petrol Products Inc. A Bruker Vertex 70 Fourier-Transform Infrared Spectrometer (FTIR) was used to characterize the grinding aid in the range of $4000\text{--}400 \text{ cm}^{-1}$.

Figure 3 shows the FT-IR spectrum of the grinding aid. Glycerin is a complex organic material with different types of polar groups. There are evident O-H stretching vibration peaks at $3600\text{--}3200 \text{ cm}^{-1}$ and the contribution of the broadband of -OH with absorption varying between 3000 and 3500 cm^{-1} was also detected. These polar hydroxyl groups in its structure provide good grinding performance. C-H stretching vibrations are observed at a wave number of 2925 cm^{-1} . A shoulder at 2853 cm^{-1} is attributed to the C-H symmetrical stretching vibration of the aliphatic CH₂ group (Zhang et al., 2016), the band observed at $1740\text{--}1653 \text{ cm}^{-1}$ stands for C=O stretching vibrations found in aromatic groups, and the obvious stretching vibration of the free fatty acid carbonyl group is observed at $1030\text{--}1200 \text{ cm}^{-1}$.

**Figure 3.** FT-IR spectrum of the grinding aid

1.2. Methods

Marble wastes were ground in a type of a Standard-01 laboratory batch mill produced by Union Process (USA) (Figure 4). Table 2 summarizes the technical specifications of the stirred ball mill. The grinding tank is equipped with a water jacket to ensure cooling. It is necessary to eliminate the heat produced in the course of grinding with circulating cooling water via the grinding container jacket. A Rev 2580 voltomat-meter (Rev Ritter GmbH, Deutschland) was utilized to measure the energy the mill consumed. Table 3 summarizes the experimental conditions.

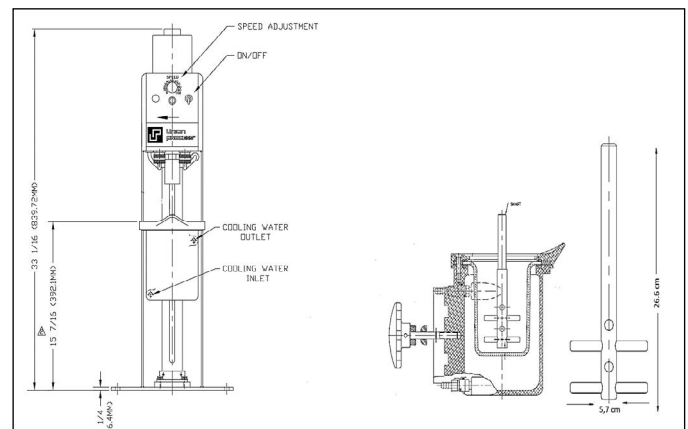
**Figure 4.** Laboratory-scale vertical stirred ball mill

Table 2. Technical specifications of the vertical stirred ball mill

Property	Value
Motor speed (max.)	600 rpm
Tank height	12.3 cm
Tank diameter	8.04 cm
Shaft type	Pin
Shaft length	26.6 cm
Number of pins	4

Table 3. Experimental conditions used in the dry grinding of marble wastes

Parameter	Value
Ball filling ratio, (J)	65
Powder filling ratio, (fc)	0.125
Grinding time, (min)	75
Mill speed, (rpm)	600
Ball size distribution	3 mm (50%) and 5 mm (50%)
Grinding aid dosage, (by weight %)	0, 0.25, 0.5, 1, and 2

Equation 1 is used to calculate the ball filling ratio (J). This parameter indicates how much of the volume is filled with media using a bed porosity of 0.4 (Austin et al., 1984); the value equals 100%.

$$J = \frac{\text{Mass of media (gr)}/\text{Density}(\text{gr}/\text{cm}^3)}{\text{Mill volume (cm}^3)} \times \frac{1.0}{0.6} \quad (1)$$

Likewise, the ratio of the mill volume filled with solids ratio (fc) is explained by Equation 2.

$$fc = \frac{\text{Mass of powder (gr)}/\text{Powder density}(\text{gr}/\text{cm}^3)}{\text{Mill volume (cm}^3)} \times \frac{1.0}{0.6} \quad (2)$$

The measurement of the energy consumption in the course of the dry grinding process was performed for the purpose of assessing the efficiency of the grinding process.

$$E_m(kWh/t) = \frac{E - E_0}{m_p} \quad (3)$$

Where denotes the product mass of marble wastes, E is the energy used at the time t, and is the no-load energy.

2. Results and discussion

2.1. Product fineness

First, the influence of glycerin dosage on grinding was investigated under constant mill parameters, as shown in Figure 5, using the particle sizes d_{50} for calcitic marble (left side) and dolomitic marble (right side).

Figure 5 obviously shows that with the addition of glycerin, the d_{50} size becomes narrower in comparison with the no-aid condition. Glycerin consists of a chain of three car-

bon atoms where each carbon atom is bonded to a hydrogen atom (+H) and a hydroxyl group (-OH). Furthermore, it is all highly adsorbed by polar -OH groups. However, the d_{50} size increased beyond the dosage of 0.5% for calcitic marble and dolomitic marble. Generally, this is not surprising since this phenomenon is called “negative grinding,” known as the re-agglomeration of fine particles (Hasegawa et al., 2001). Similar results to this study were obtained in the studies by Katircioğlu-Bayel and Toghan (2022) on waste eggshell, Toraman (2012) and Çayirli (2018) on calcite, and Oksuzoğlu and Ucurum (2016) on gypsum.

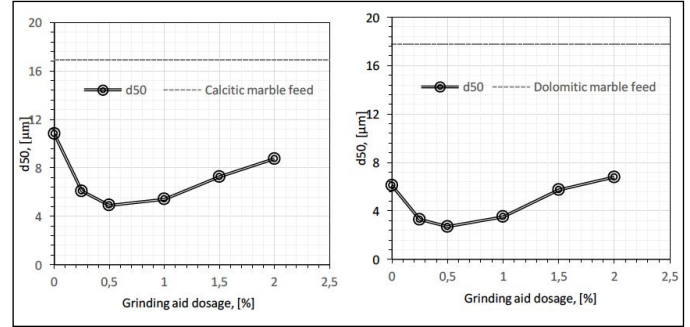


Figure 5. Influence of the grinding aid concentration on the d_{50} size

Except for the d_{50} size, Figure 6 shows the influence of the grinding aid dosage on size reduction (F_{90}/P_{90}) for calcitic marble (left side) and dolomitic marble (right side). Glycerin had higher size reduction ratios than the no-aid condition. The size reduction ratio increases with an increasing dosage up to 0.5% for calcitic and dolomitic marble and then decreases. As the grinding aid dosage increases (after optimal dosage), the distance between particles changes with the contribution of repulsive and attractive forces and the thickening of the adsorption layer (Prziwara et al., 2018).

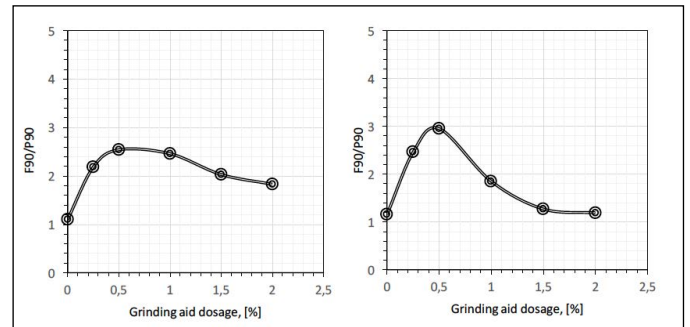


Figure 6. Influence of the grinding aid concentration on the d_{50} size

2.2. Grinding media coating

The coating of grinding media with waste products was detected by weighing it after 30 s of dry sieving. Figure 7 shows the coating values according to the decrease and increase of coating on grinding media.

The grinding media coating without any additives was 83 and 15 g/m² for calcitic and dolomitic marbles, respectively. The results for all dosages show that the coating of grinding media with the product decreased dramatically.

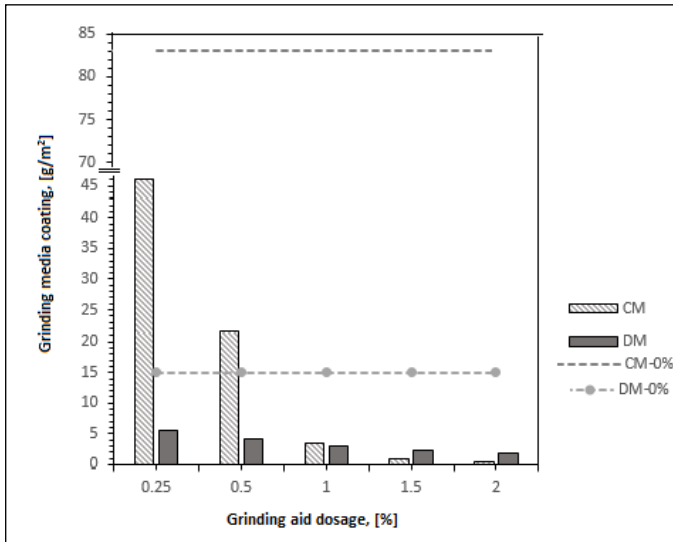


Figure 7. Grinding media coating of calcitic and dolomitic marble

2.3. Energy consumption

It is known that the fineness of the product obtained as a result of grinding is proportional to the energy consumed. One way to increase the grinding energy efficiency in ultra-fine grinding is to use grinding additives. Tuunila (1997), Wang and Forssberg (1995), Zheng et al. (1997), Choi et al. (2010), and Choi and Wang (2007) planned to increase the grinding and energy efficiency with the addition of appropriate chemicals. The results obtained in this study are in agreement with previous studies in the literature.

The influence of the grinding aid dosage on energy consumption was investigated, as shown in Figure 8, for calcitic marble (left side) and dolomitic marble (right side).

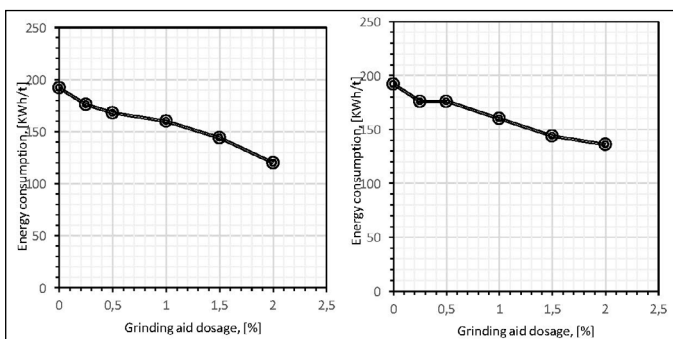


Figure 8. Energy consumption of calcitic and dolomitic marble

Concerning the experimental results, energy consumption for calcitic marble, which was 192 kWh/t without additives, decreased to 120 kWh/t with the use of glycerin. Thus, 72 kWh/t energy savings were achieved. The energy consumption for dolomitic marble, which was 192 kWh/t without additives, decreased to 136 kWh/t. Thus, 56 kWh/t energy savings were achieved in dolomitic marble. The specific energy consumption improved with grinding additives (Katırcıoğlu-Bayel, 2018).

Conclusions

This study identified the effects of glycerin on product fineness, energy consumption, and grinding media coat-

ing. Based on the results, the following conclusions can be drawn:

(1) Adding glycerin improved the product fineness compared to the no-aid condition. The increase in grinding aid dosage from 0 to 0.5% decreased the d_{50} particle size from 10.3 to 4.9 μm for calcitic marble and from 6.1 to 2.7 μm for dolomitic marble. However, the re-agglomeration phenomenon was observed again, and the d_{50} particle size was increased. The same results were obtained for the size reduction ratio.

(2) The grinding media coating without any additives was 83 and 15 g/m² for calcitic and dolomitic marbles, respectively. The results for all concentrations show that the coating of grinding media with the product decreased dramatically.

(3) The specific energy consumption improved with grinding additives. Moreover, as the amount of grinding aids increased, energy consumption decreased. This positive impact of grinding aids on energy consumption could be attributed to the ease of powder flow.

With this study, it was understood that calcitic and dolomitic marble samples could be dry ground to ultrafine sizes in a laboratory-scale vertical stirred mill. As a result, unrefined glycerin was identified as an excellent quality additive improving the grinding performance of marble waste. A study was carried out to shed light on the fact that it could be used in alternative products in grinding processes where imported grinding chemicals were generally used.

Acknowledgment

This study was supported by Niğde Ömer Halisdemir University Scientific Research Projects Coordination Unit within the scope of project number MMT 2020/3. The author would like to thank Kolza Biodizel Fuel and Petrol Products Inc. for providing unrefined glycerin.

References

- Alyamac, K.E., Ince, R. 2009. A preliminary concrete mix design for SCC with marble powders. *Construction and Building Materials*. 23(3), 1201-1210. <https://doi.org/10.1016/j.conbuildmat.2008.08.012>
- Austin, L.G., Klimpel, R.R., Luckie, P.T. 1984. *Process engineering of size reduction: Ball milling*. SME, New York, 561 p.
- Cayirli, S. 2018. Influences of operating parameters on dry ball mill performance. *Physicochemical Problems of Mineral Processing*. 54(3), 751-762. <https://doi.org/10.5277/ppmp1876>
- Chi, Z., Pyle, D., Wen, Z., Frear, C., Chen, S.A. 2007. Laboratory study of producing doco-sahexaenoic acid from biodiesel-waste glycerol by microalgal fermentation. *Process Biochemistry*. 42(11):1537-45. <https://doi.org/10.1016/j.procbio.2007.08.008>
- Choi, H.K., Wang, L. 2007. A quantitative study of grinding characteristics on particle size and grinding consumption energy by stirred ball mill. *Korean Journal of Materials Research*. 17(10), 532-537. <https://doi.org/10.3740/MRSK.2007.17.10.532>
- Choi, H.K., Lee, W., Kim, D.U., Kumar, S., Kim, S.S., Chung, H.S., Kim, J.H., Ahn, Y.C., 2010. Effect of grinding aids on the grinding energy consumed during grinding of calcite in a stirred ball mill. *Minerals Engineering*. 23, 54-57. <https://doi.org/10.1016/j.mineng.2009.09.011>
- DPT, 2001. Madencilik Özel İhtisas Komisyonu Raporu, Endüstriyel Hammaddeler Alt Komisyonu Genel Endüstri Mineralleri I, Çalışma Grubu

- Raporu. DPT:2618- ÖİK:629, 99sf.
- El-Shall, H., Somasundaran, P. 1984. Physico-chemical aspects of grinding: a review of use of additives. *Powder Technology*. 38, 275-293. [https://doi.org/10.1016/0032-5910\(84\)85009-3](https://doi.org/10.1016/0032-5910(84)85009-3)
- El-Sherbiny, S., El-Sheikh, S. M., Barhoum, A. 2015. Preparation and modification of nano calcium carbonate filler from waste marble dust and commercial limestone for papermaking wet end application. *Powder Technology*. 279, 290-300. <https://doi.org/10.1016/j.powtec.2015.04.006>
- Fuerstenau, D.W. 1995. Grinding aids. *Kona*. 13, 5-18.
- Gao, X., Yang, Y., Deng, H. 2011. Utilization of beet molasses as a grinding aid in blended cements. *Construction and Building Materials*. 25(9), 3782-3789. <https://doi.org/10.1016/j.conbuildmat.2011.04.041>
- Hasegawa, M., Kimata, M., Shimane, M., Shoji, M., Tsuruta, M. 2001. The effect of liquid additives on dry ultrafine grinding of quartz. *Powder Technology*. 114, 145-151. [https://doi.org/10.1016/S0032-5910\(00\)00290-4](https://doi.org/10.1016/S0032-5910(00)00290-4)
- Karinen, R.S., Krause, A.O.I. 2006. New biocomponents from glycerol. *Applied Catalysis A: General*. 306, 128-133. <https://doi.org/10.1016/j.apcata.2006.03.047>
- Katırcıoğlu-Bayel, D. 2018. The Effect of Grinding Additives on Stirred Media Milling of Talc. *International Journal of Innovative Science, Engineering & Technology*. 5(7), 36-39.
- Katırcıoğlu-Bayel, D., Toghan E.W. 2022. Karıştırılmalı Bilyalı Değirmende Biyo-Dolgu Malzemesi Üretiminde Öğütme Yardımcılarının Etkisi. *Konya Mühendislik Bilimleri Dergisi*. 10(1), 61-71.
- Leoneti, A.B., Aragão-Leoneti, V., De Oliveira, S.V.W.B. 2012. Glycerol as a by-product of biodiesel production in Brazil: alternatives for the use of unrefined glycerol. *Renewable Energy*. 45, 138-145. <https://doi.org/10.1016/j.renene.2012.02.032>
- Li, H., Jiang, Z., Yang, X., Yu, L., Zhang, G., Wu, J., ve Liu, X. 2015. Sustainable resource opportunity for cane molasses: Use of cane molasses as a grinding aid in the production of portland cement. *Journal of Cleaner Production*. 93, 56-64. doi: <https://doi.org/10.1016/j.jclepro.2015.01.027>
- Li, H., Zhao, J., Huang, Y., Jiang, Z., Yang, X., Yang, Z., Chen, Q., 2016. Investigation on the potential of waste cooking oil as a grinding aid in Portland cement. *Journal of environmental management*. 184, 545-551. <https://doi.org/10.1016/j.jenvman.2016.10.027>
- Locher, F.W., Seebach, H.M. 1972. Influence of adsorption on industrial grinding. *Ind. & Eng. Chem. Des. Develop.* 11(2), 190-197.
- Mymrin, V.A. 1997. Environment protection by industrial wastes utilization for engineering geology goals. *Engineering Geology and the Environment*. 2027-2031.
- Nayak, S. K., Satapathy, A., Mantry, S. 2022. Use of waste marble and granite dust in structural applications: A review. *Journal of Building Engineering*. 46, 103742. <https://doi.org/10.1016/j.job.2021.103742>
- Oksuzoglu, B., Ucurum, M. 2016. An experimental study on the ultra-fine grinding of gypsum ore in a dry ball mill. *Powder Technology*. 291, 186-192. <https://doi.org/10.1016/j.powtec.2015.12.027>
- Orumwense, O.A., Forssberg, E. 1992. Superfine and ultrafine grinding-a literature survey. *Mineral Processing and Extractive Metallurgy Review*. 11, 107-127. <https://doi.org/10.1080/08827509208914216>
- Prziwara, P., Breitung-Faes, S., Kwade, A. 2018. Impact of grinding aids on dry grinding performance, bulk properties and surface energy. *Advanced Powder Technology*. 29(2), 416-425. <https://doi.org/10.1016/j.apt.2017.11.029>
- Sabine, S., 2013. The role of universities in fostering sustainable development at the regional level. *J. Clean. Prod.* 48, 74-84. <https://doi.org/10.1016/j.jclepro.2013.01.029>
- Toraman, O.Y. 2012. Effect of chemical additive on stirred bead milling of calcite powder. *Powder Technology*. 221, 189-191. <https://doi.org/10.1016/j.powtec.2011.12.067>
- Tunc, E.T. 2018. Investigation of the abrasion resistance of the quartzitic natural aggregate for different test parameters. *Qualitative Studies*. 13(2), 57-67.
- Tuunila, R., 1997. Ultrafine grinding of FGD and phosphogypsum with an attrition bead mill and a jet mill: optimisation and modelling of grinding and mill comparison. Thesis (PhD). Lappeenranta University of Technology.
- Wang, Y. and Forssberg, E. 1995. Dispersants in stirred ball mill grinding. *KONA Powder and Particle Journal*. 13, 67-77. <https://doi.org/10.14356/kona.1995011>
- Zhang, L., Luo, M., Sun, S., Ma, J., & Li, C. 2010. Effect of surface structure of nano-CaCO₃ particles on mechanical and rheological properties of PVC composites. *Journal of Macromolecular Science, Part B*. 49(5), 970-982. <https://doi.org/10.1080/00222341003609336>
- Zhang, Y., Fei, A., Li, D. 2016. Utilization of waste glycerin, industry lignin and cane molasses as grinding aids in blended cement. *Construction and Building Materials*. 123, 785-791. <https://doi.org/10.1016/j.conbuildmat.2016.07.034>
- Zheng, J., Harris, C.C., Somasundaran, P. 1997. The effect of additives on stirred media milling of limestone. *Powder Technology*. 91(3), 173-179. [https://doi.org/10.1016/S0032-5910\(96\)03236-6](https://doi.org/10.1016/S0032-5910(96)03236-6)



Analysis of Bottleneck using Mine Production Index and Ishikawa Diagram: A Case of Indian Coal Mine

Sorokhaibam Khaba^{a,*}

^a Institute of Management Technology Dubai, Dubai-345006, United Arab Emirates.

Received: 10 August 2022 • Accepted: 18 July 2023

A B S T R A C T

The traditional way of coal production and management is still predominant in the Indian coal mining industry which has led to a widespread waste of resources both materials and humans. Operational loss of the mining machinery and equipment is one of the key factors for the low performance and productivity of mines. This research presents an application of the integrated approach of the Mine Production Index (MPI) and Ishikawa Diagram in an Indian coal mine to study the bottleneck equipment in the mining operation among the fleet of shovels, trucks (dump trucks), and dozers. Mine Production Index (MPI) identifies the bottleneck equipment in the mining operation, and Ishikawa Diagram presents the Root Cause Analysis of bottleneck equipment. The Fuzzy Analytical Hierarchy Process (FAHP) is used to determine weights for MPI calculation using information gathered from a group of 11 experts through structured interviews. The study found that the dozer fleet is the bottleneck equipment and the ineffectiveness of the dozer fleet can be grouped into 4 categories as enumerated on the Ishikawa diagram. The study proposes that the ineffectiveness of the dozer fleet can be improved with an increase in its performance rate. The study is based on the judgments of the experts for the case mine, which may limit the external validity. This paper is an original contribution to the analysis of mining equipment using the Mine Production Index and Ishikawa Diagram in an Indian coal mine.

Keywords: Indian Coal Mining Industry; Mine Production Index; Ishikawa Diagram; Fuzzy Analytical Hierarchy Process.

Introduction

The traditional way of the coal production process is still predominant in the Indian coal mining industry which has led to widespread waste of resources for both materials and humans. Operational losses for machinery and equipment such as losses due to breakdown, waiting time during set-up, adjustments and small stops, defects, over-processing, and rework are the main factors affecting the performance and productivity of the machines and equipment. Operational loss is one of the major factors for the low productivity of the Indian coal mining industry despite augmenting investment, introducing updated equipment, and improving labor intensity. The Indian coal mining industry is no exception; despite augmenting investment, introducing updated equipment, and improving the labor intensity in recent years. The management of bottlenecks is key to reducing costs and remaining competitive in the global market. The concept of “lean

mining” in the Indian coal mining industry is put forward in this paper through the application of the Mine Production Index (MPI) and Root Cause Analysis (RCA) using the Cause and Effect Diagram (Ishikawa diagram). Although there is considerable literature available about lean application in the mining industry, a few authors address the practical applications of lean in mines.

MPI addresses the issues of poor performance and low productivity by identifying bottleneck equipment in mining operations. MPI was introduced in 2014 and is an extension of Overall Equipment Efficiency (OEE) with the introduction of weight for each factor considering some operational constraints in the mining industry (Lanke *et al.*, 2014). OEE is a Key Performance Index (KPI) that can be used to determine the overall performance of an industry. Availability, utilization, and performance rate are the parameters that form the product of MPI and are calculated as follows:

* Corresponding author: prinshaba@gmail.com • <https://orcid.org/0000-0002-5608-0180>

$$= (Av^a \times Ut^b \times Pp^c) \tag{1}$$

where Av is Availability, Ut is utilization and Pp is performance of the equipment.

a, b, and c are weights such that $0 < a, b, c < 1$ and $\sum(a, b, c) = 1$

Several Multi-Criteria Decision Making(MCDM) tools such as the Analytical Hierarchy Process (AHP), Fuzzy Analytical Hierarchy Process(FAHP), Weighted Sum Model(WSM),Technique for Order of Preference by Similarity to Ideal Solution(TOPSIS),Elimination and Choice Expressing REality (ELECTRE), etc. can be used for determining the weights of the factors used in the MPi formula. In this study, Fuzzy AHP is used to calculate the weights of the factors for calculating the MPi of mining machines to study its overall effectiveness.

There are many productivity-related issues in the mining industry due to the inherent mining work environment and varying degrees of assignable causes such as inefficiency of manpower or machinery. RCA for productivity-related issues is an essential step for any multi-stage production process (Wilson *et al.*, 1993). RCA is a step-by-step process of identifying causal factors using comprehensive and system-based review techniques aimed to provide the focal root causes of problems and to develop action plans with measurement strategies to resolve the problem. Cause and Effect Diagram (CED), also known as Fishbone or Ishikawa Diagram, is an RCA tool that can be used to identify and organize the possible causes for a particular single effect (Wilson *et al.*, 1993).

The main objectives of this paper are:

- To identify the bottleneck equipment in a mining operation in an Indian coal mine through the application of MPi.
- RCA of bottleneck equipment using a cause and effect diagram.

The subsequent sections present a literature review on the background of MPi to concisely describe its key advantages over OEE. This is followed by the background of AHP, Fuzzy AHP, Root cause Analysis, and Ishikawa diagram. In section 3, the methodology adopted for the study is discussed where the stepwise determination of weights of the factors using FAHP is shown which is followed by steps of cause and effect diagram in the subsequent section. The next section presents the illustration of a case study. The final section presents discussions on the key results followed by the conclusions, limitations, and directions for future research.

2. Literature Review

2.1. Mine Production Index

Mine Production Index is an operational measure for the mining sector which is an extension of the OEE concept by assigning different weights to the traditional OEE components (Lanke *et al.*, 2014). It helps in identifying the bottleneck and its root causes in mining operations reliably. The literature review reveals that MPi evaluates not only effective equipment but also the effect of assessment factors on the effectiveness (Lanke *et al.*, 2016). Availability, utilization, and performance rate, which are considered important criteria for determining mining equipment productivity, form the product of.

The availability rate is defined as the ratio of the available shift/planned time for production to the total available shift/planned time (Elevli and Elevli, 2010). It considers the downtime such as breakdowns and waiting times due to set-ups, maintenance actions, adjustments, etc.

$$\text{Availability} = \frac{\text{Total available shift or planned time for production} - \text{total downtime}}{\text{Total available shift or planned time for production}} \tag{2}$$

Performance rate is defined as the ratio of actual output from a machine to the rated output (Elevli and Elevli, 2010). It is used for the assessment of decreased performance and operational efficiency of machines due to reduced machine speed or delays in cycle time, etc.

$$\text{Performance rate} = \frac{\text{Actual output from a machine (satisfying quality standard)}}{\text{Rated output (during the time machine is operating)}} \tag{3}$$

The utilization of equipment is defined as the ratio of the time in hours the machine is used in a year to the total hours which can be either total annual Scheduled Shift Hours (SSH) or total Machine Available Hours (MAH) in a year (Arputharaj, 2015).

$$\text{Utilisation} = \frac{\text{Actual hours used in a year}}{\text{Total annual SSH or total MAH in a year}} \tag{4}$$

2.2. Analytic Hierarchy Process

The Analytic Hierarchy Process was developed by Saaty (1980) and is one of the most widely used MCDM tools to assist complex decision-making. AHP is a method that structures the decision problem into a hierarchical level by eliciting pair-wise comparison that indicates the relative importance of all criteria or alternatives using a 9-point scale (Saaty, 1980). AHP has been applied in various decision-making environments like to prevent child sexual abuse in schools (Lundberg and Dangel, 2019); develop weighting system (Kamaruzzaman *et al.*, 2018); management effectiveness (Pendred *et al.*, 2016), and machine tool configurations (Farhan *et al.*, 2016).

2.3. Fuzzy Analytic Hierarchy Process

In AHP, the relationships of the factors are based on the subjective judgment of the experts which are expressed in crisp values. Thus, the relationships may be imprecise as it is hard to estimate our judgments by specific numerical values and the results may misguide in decision-making. Although AHP is an accomplished tool for the assessment of problems, Fuzzy theory can be integrated into AHP to increase the sensitivity of the AHP method with fuzziness situations. The combination of fuzzy concepts and AHP is called fuzzy AHP (FAHP).

2.3.1. Fuzzy Set Theory

The fuzzy set was introduced by Zadeh in 1965 (Zadeh,1965) as an extension of the classical notion of a set whose elements have degrees of membership. A classical bivalent set, called a crisp set, evaluates in binary terms according to a condition i.e. an element either belongs or does not belong to the set while a fuzzy set defines a degree of belonging to the possible individual in the universe of discourse by assigning a value representing its degree of membership in the fuzzy set. So, fuzzy set theory can be used in solving complex problems to measure uncertainty in human insight and implication.

2.3.2. Triangular Fuzzy Number

Let X be a universe of discourse having its generic elements Y, or $Y = \{y_1, y_2, y_3, \dots, y_n\}$. A fuzzy set F in Y is characterized by a membership function, (Y), which maps Y to the membership space

[0, 1]. A fuzzy number F is defined as a triangular fuzzy number (TFN) parameterized by the triplet (p, q, r) with peak value q, left width p > 0, and right width r > 0, if its membership function has the following form (Khaba and Bhar, 2017; Cheng, 1999):

$$\begin{aligned} \mu_F(Y) &= (y-p)/(q-p) \quad p \leq y \leq q \\ &= (\beta-p)/(\beta-q) \quad q \leq y \leq r \end{aligned} \tag{5}$$

The membership function is defined in Figure 1.

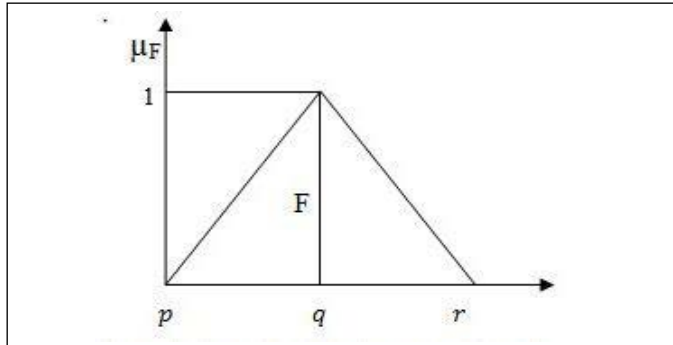


Figure 1. A triangular fuzzy number F.

Fuzzy AHP has been applied in various decision-making environments like raw material criticality assessment (Kim *et al.*, 2019); network access of mobile applications (Mowafi *et al.*, 2019); health symptom checking system (Huang *et al.*, 2018); clinical decision support system (Nazari *et al.*, 2018); prioritizing the solutions of lean implementation (Belhadi *et al.*, 2017); water loss management (Zyoud *et al.*, 2016); analysis of reverse logistics implementation (Prakash *et al.*, 2015); machine tool evaluation (Ayag and Gurcan Ozdemir, 2012); failure modes and effects analysis (Kutlu and Ekmekçioğlu, 2012); supplier selection (Beik-khakhian *et al.*, 2015; Shaw *et al.*, 2012, Yu *et al.*, 2012); partner's selection within a green supply chain (Lee *et al.*, 2011); mining equipment selection (Kesimal and Bascetin, 2002). The extent analysis method is one of the extensively used fuzzy weighing and prioritizing methods due to its simplicity and efficiency (Chang, 1996) while the centre of gravity is one of the widely used methods of defuzzification (Kang *et al.*, 2010), and both the approaches are applied in this study. Other methods include centroid (Lee *et al.*, 2010) and α -cut (Buckley and Qu, 1990).

2.4. Cause and Effect Diagram

Cause and Effect Diagram (CED), 5 Whys, Interrelationship Diagram (ID), Multi Vari Analysis, and the Current Reality Tree (CRT) are some of the RCA tools that help in identifying the root causes of problems (Duggett, 2004). RCA tools have been used for studying failure to improve patient safety (Kellogg *et al.*, 2017); factors contributing to cancer-related suicide (Aboumrada, *et al.*, 2018). Cause and effect diagram (CED), also known as Fishbone or Ishikawa Diagram is used to identify and organize the possible causes for a particular single effect (Wilson *et al.*, 1993). In the CED, the potential causes are often organized into 4 key groups for identifying the root cause- manpower, materials, machinery, and methods in the manufacturing sector while people, policies, equipment, and procedures for the service sector. Many studies have used the Ishikawa diagram for diagnosing the root causes of different industrial problems such as productivity losses in mining equipment (Papic *et al.*, 2016); minimizing rejection of raw materials (Ahmed and Ahmad, 2011), equipment unreliability (Sharma and Sharma,

2010), etc. The drawbacks of the Ishikawa diagram are highly expert-driven, considerable manpower requirements in the form of expert teams to conduct the analysis, and insufficient explanation of possible strategies for mitigating the root causes (Guerin, 2015; Reid *et al.*, 2012).

3. Research Methodology

In this study, an integrated approach of FAHP for MPi calculation and CED for RCA has been used. The structured interview is used to collect information and knowledge from the experts for developing the pairwise comparison matrices to determine the weights for MPi evaluation of mining machines. A total number of 11 experts, 8 from the mining sector (from the case study mine) and 3 from academic institutions with substantial experience were consulted and asked to respond to the importance of each factor on a scale of 1 to 9 using an interview questionnaire. In the next stage, the cause and effect analysis method are done to integrate experts' knowledge for a possible solution to the bottleneck. In this study, cause and effect analysis is done through personal observations, consensus building, and semi-structured interviews with a cross-functional team of 15 employees from different departments of the mine.

3.1. Steps of Fuzzy AHP

The various steps adopted in this study are discussed below:

Step 1: The first step of FAHP is to construct a pairwise comparison matrix with the data collected from z experts for the n factors using Saaty's 9-point scale. For each expert, an nxn non-negative pairwise comparison matrix is constructed. Each pairwise comparison matrix is also checked for consistency.

Step 2: The pairwise comparison matrices are converted into fuzzy comparison matrices using the corresponding characteristic (membership) function as shown in Table 1.

Table 1. Characteristic function of the fuzzy numbers.

Fuzzy number	Characteristic (membership) function
$\tilde{1}$	(1, 1, 2)
\tilde{x}	(x-1, x, x + 1) for x = 2, 3, 4, 5, 6, 7, 8
$\tilde{9}$	(8, 9, 9)
$1/\tilde{1}$	(1/2, 1, 1)
$1/\tilde{x}$	{1/(x+1)}, {1/x}, {1/(x - 1)} for x = 2, 3, 4, 5, 6, 7, 8
$1/\tilde{9}$	(1/9, 1/9, 1/8)

The membership function is TFN and thus requires fuzzy aggregation to achieve a favorable result from the responses of experts. In our study, fuzzy comparison matrices are aggregated by the geometric mean method. The aggregated fuzzy comparison matrix for Z number of experts is represented by $A_{ij} = (p_{ij}, q_{ij}, r_{ij})$, where

$$p_{ij} = \left(\prod_{t=1}^Z p_{ij,t} \right)^{\frac{1}{Z}}, \forall t = 1, 2, 3 \dots, Z \tag{6}$$

$$q_{ij} = \left(\prod_{t=1}^Z q_{ij,t} \right)^{\frac{1}{Z}}, \forall t = 1, 2, 3 \dots, Z \tag{7}$$

$$= \left(\prod_{t=1}^Z r_{ijt} \right)^{\frac{1}{Z}}, \forall t = 1, 2, 3, \dots, Z \tag{8}$$

Step 3: The next step is the defuzzification of the aggregated fuzzy comparison matrix into crisp scores using the defuzzification method for testing consistency. In this study, the Centre of Area (COA) method is applied for defuzzification by using the following equation:

$$F_i = \frac{[(r_i - p_i) + (q_i - r_i)]}{3} + p_i \tag{9}$$

Step 4: Fuzzy synthetic extent analysis is used for determining the weight of the aggregated fuzzy comparison matrix. According to Chang (1996), if $X = \{x_1, x_2, x_3, \dots, x_n\}$ be the objects set, $U = \{u_1, u_2, \dots, u_m\}$ be a goal set and $M_{gi}^1, M_{gi}^2, \dots, M_{gi}^m$ be the values of extent analysis of i^{th} object for m goals, then the fuzzy synthetic value of the i^{th} object can be determined by using equations (10) - (12) as follows:

$$F_i = \sum_{j=1}^m M_{gi}^j \otimes \left[\sum_{i=1}^n \sum_{j=1}^m M_{gi}^j \right]^{-1} \tag{10}$$

$$\left[\sum_{i=1}^n \sum_{j=1}^m M_{gi}^j \right]^{-1} = \left(\left[\sum_{i=1}^n \sum_{j=1}^m p_{ij} \right]^{-1}, \left[\sum_{i=1}^n \sum_{j=1}^m q_{ij} \right]^{-1}, \right. \tag{11}$$

$$\left. \left[\sum_{i=1}^n \sum_{j=1}^m r_{ij} \right]^{-1} \right) \tag{12}$$

Step 5: After calculating the fuzzy synthetic value (F_i) for the i^{th} object, the F values are compared.

Consider two convex fuzzy numbers $F_1 = (p_1, q_1, r_1)$ and $F_2 = (p_2, q_2, r_2)$ as shown in Figure 2. The degree of possibility of F_2 greater than F_1 is defined as

$$V(F_2 \geq F_1) = 1 \text{ if } p_1 \geq p_2, q_1 \geq q_2 \text{ and } r_1 \geq r_2 \tag{13}$$

$$\text{Or } V(F_2 \geq F_1) = \text{hgt}(F_1 \cap F_2) =$$

$$(p_1 - r_2) / (q_2 - r_2) - (q_1 - p_1) \tag{14}$$

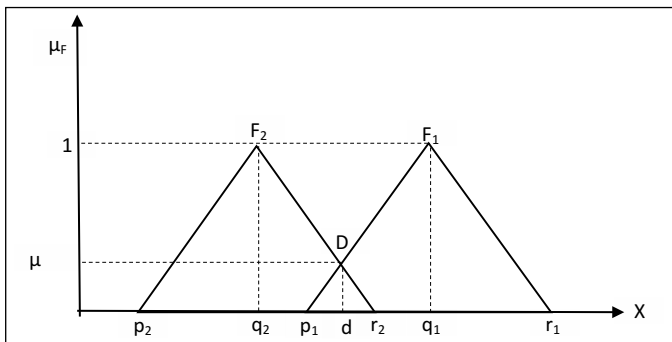


Figure 2. Two triangular Fuzzy numbers F_1 and F_2 (Cheng, 1999).

The degree of possibility of a convex fuzzy number F greater than k convex fuzzy numbers is defined as

$$V(F \geq F_1, F_2, \dots, F_k) = V[(F \geq F_1) \text{ and } (F \geq F_2) \text{ and } (F \geq F_3) \dots (F \geq F_k)]$$

$$= \min V(F \geq F_i) \forall i = 1, 2, \dots, k \tag{15}$$

$$\text{Consider } d(F_i) = \min V(F_i \geq F_k) \forall k = 1, 2, \dots, t \text{ and } k \neq i \tag{16}$$

The weight vector is calculated as

$$\bar{W} = [(d(F_1), d(F_2), \dots, d(F_t))]^T \text{ where } F_i (i = 1, 2, \dots, t) \text{ are elements} \tag{17}$$

Step 6: The priority weight vector is obtained after normalization as follows $W = [(d'(F_1), d'(F_2), \dots, d'(F_t))]^T =$

$$(w_1, w_2, w_3, w_4, \dots, w_t) \text{ where } W \text{ is a nonfuzzy number} \tag{18}$$

3.2. Calculation of MPI

MPI is calculated using Equation 1 by assigning the weights for each parameter that has been identified using the FAHP.

3.3. Steps of Cause and Effect Diagram

The steps of the CED adapted from the literature (Ishikawa, 1990; Sharma and Sharma, 2010; Papic et al., 2016) are shown below:

1. Select a multi-disciplinary Cross-Functional Team (CFT) or inter-departmental team
2. Define the problem
3. Collect data implementing the '3W2H' tool (what, when, where, how, how much) to categorize the characteristics of the cause
4. Study every possible causal factor
5. Check all the consistent and reliable causes and eliminate all inconsistent causes, thus identifying the root cause(s)

4. Case Study

The study of the application of MPI for evaluation of the mining equipment productivity is carried out in an Indian open-pit mine operated in eastern India. The mine is operated for 24 hours 7 days a week in 3 shifts of 8 hours each day. The poor performance of key mining machinery is the main problem of this mine in the production process resulting in low productivity. The purpose of using MPI in the process is to identify the significant bottleneck and measure the effectiveness of the machine which is followed by root cause analysis of the bottleneck equipment. The productivity of the fleet of 3 mining equipment is being studied using MPI. The data collection for availability (total working duration, standby hours), performance, and utilization (idle time and downtime time, etc.) of the shovel, truck, and dozer was performed for a period of 12 months from November 2015 to October 2016. The production performance is measured in terms of total output by each fleet of equipment operated in the mine and hence the output data are also collected. In this mine, the shovel fleet consists of 14 shovels, a dozer fleet of 17 dozers and the trucks fleet consists of 38 trucks with three different capacities.

4.1. Data Collection and Development of the Hierarchy

In this study, a structured interview was used to collect information and knowledge from the experts for developing the pairwise comparison matrices to determine the weights for MPI evaluation of mining machines. An interview questionnaire was designed for data collection and evaluation to ensure the content validity of the questionnaire. A total number of 11 experts, 8 from the mining sector (from the case study mine) and 3 from academic institutions with substantial experience were consulted and asked to respond to the importance of each factor on a scale of 1 to 9 using an interview questionnaire followed by elicitation of experts and semi-structured interviews with a cross-functional team of 15 employees from different departments of the mine and personal observations for the cause and effect analysis for a possible solution to the bottleneck.

4.1.1. Development of the Pairwise Comparison Matrix

The first step of FAHP is to construct a pairwise comparison matrix with the data collected from 11 experts for the 3 factors using a comparison scale of 1-9. For each expert, a 3 x 3 non-negative pairwise comparison matrix is constructed. Thus, the importance levels were obtained for availability, performance, and utilization. Each pairwise comparison matrix is also checked for consistency. The pairwise comparison matrices are converted into fuzzy comparison matrices using the corresponding characteristic (membership) function using Table 2.

4.1.2. Integration of the Fuzzy Comparison Matrices:

The fuzzy comparison matrices from 11 experts are incorporated into a final comparison matrix by the geometric mean process which is shown in Equations (6), (7), and (8). For example, the aggregated fuzzy number F_{12} in the fuzzy comparison matrix for the dozer is represented as, (p_{12}, q_{12}, r_{12}) , where,

$$p_{12} = (4 * 2 * 1 * 2 * 4 * 1 * 4 * 2 * 2 * 1 * 1)^{1/11} = 1.88$$

$$q_{12} = (5 * 3 * 2 * 3 * 5 * 2 * 5 * 3 * 3 * 2 * 2)^{1/11} = 2.98$$

$$r_{12} = (6 * 4 * 3 * 4 * 6 * 3 * 6 * 4 * 4 * 3 * 3)^{1/11} = 4.02$$

The aggregated fuzzy comparison matrices for the shovel, truck, and dozer are shown in Tables 2, 3, and 4, respectively.

Table 2. Aggregated fuzzy comparison matrices for shovel.

	Availability	Utilization	Performance
Availability	(1,1,1)	(1.95,2.9,4.02)	(1.29, 2.32,3.33)
Utilization	(0.25,0.33,0.51)	(1,1,1)	(0.33,0.50,0.90)
Performance	(0.30,0.43,0.78)	(1.11, 2,3.03)	(1,1,1)

Table 3. Aggregated fuzzy comparison matrices for truck.

	Availability	Utilization	Performance
Availability	(1,1,1)	(2, 3.06,4.09)	(1.2, 2.23,3.24)
Utilization	(0.24,0.32,0.50)	(1,1,1)	(0.31,0.45,0.85)
Performance	(0.31,0.45,0.83)	(1.18, 2.21,3.23)	(1,1,1)

Table 4. Aggregated fuzzy comparison matrices for dozer.

	Availability	Utilization	Performance
Availability	(1,1,1)	(1.88,2.98,4.02)	(1.07, 1.61, 2.66)
Utilization	(0.24,0.33,0.53)	(1,1,1)	(0.27, 0.37, 0.62)
Performance	(0.4,0.62,0.94)	(1.61,2.66,3.68)	(1,1,1)

4.1.3. Defuzzification of the aggregated Fuzzy Comparison Matrix

For the defuzzification of the aggregated fuzzy comparison matrix, the COA method is used. Using Equation (9), the aggregated fuzzy comparison matrix of the factors was defuzzified. Then the consistency ratio of the defuzzified integrated comparison matrix is checked.

4.1.4. Calculation of the Fuzzy Synthetic Value

The fuzzy synthetic value of assessment factors is calculated from the aggregated comparison matrix by using Equations (10) - (12). The fuzzy synthetic value of the dozer is shown below:

$$\sum_{i=i}^n \sum_{j=1}^k M_{gi}^j = (8.47, 11.57, 15.45)$$

$$F_1 = \sum_{j=1}^k M_{g1}^j \otimes \left[\sum_{i=1}^n \sum_{j=1}^k M_{gi}^j \right]^{-1}$$

$$F_1 = (3.95, 5.59, 7.68) \otimes (0.06, 0.09, 0.12)$$

$$F_1 = (0.24, 0.50, 0.92)$$

$$F_1 = (3.95, 5.59, 7.68) \otimes (0.06, 0.09, 0.12)$$

$$F_1 = (0.24, 0.50, 0.92)$$

Similarly, the fuzzy synthetic value of the remaining factors is calculated as

$$F_2 = (0.09, 0.15, 0.26) \text{ and } F_3 = (0.18, 0.39, 0.68)$$

4.1.5. Comparison of the Fuzzy Synthetic Value:

The fuzzy synthetic values of the factors are compared by using Equations (13) - (16)

The degree of possibility for the factors

$$V[(F_1 \geq F_2) \text{ and } (F_1 \geq F_3)] = 1$$

$$V[(F_2 \geq F_1)] = \frac{(0.24 - 0.26)}{(0.15 - 0.26) - (0.50 - 0.24)} = 0.054$$

$$V[(F_2 \geq F_3)] = 0.44, V[(F_3 \geq F_1)] = 0.8 \text{ and } V[(F_3 \geq F_2)] = 1$$

The degree of possibility that F_1 is greater than F_2 and F_3 is $(F_1 \geq F_1, F_2, F_3) = \min(1, 1) = 1$

$$\text{Similarly, } V(F_2 \geq F_1, F_3) = \min(0.054, 0.44) = 0.054$$

$$V(F_3 \geq F_1, F_2) = \min(1, 0.8) = 0.8$$

4.1.6. Calculation of the Weights:

- Using the possible value of the criteria, the weight of the criteria is calculated by using Equations (17) and (18):

$$W = (1, 0.05, 0.8)^T$$

$$W'_{\text{Dozer}} = (0.54, 0.03, 0.43)$$

Similarly, the weights of the assessment factors for the shovel and truck are calculated.

$$W'_{\text{Shovel}} = (0.60, 0.05, 0.354) \tag{19}$$

$$W'_{\text{Truck}} = (0.60, 0.04, 0.36) \tag{20}$$

$$W'_{\text{Dozer}} = (0.54, 0.03, 0.43) \tag{21}$$

4.2. Calculation of MPi

The information for availability, utilization, and performance of the shovel, truck, and dozer at the mine for the period under study are presented in Figures 3-5. The average percentage of availability, utilization, and performance for shovel, truck, and dozer is taken for MPi calculation. The average percentage of the

factors for each machine along with the permissible norms of the Government of India for this mine, represented within the parenthesis, is shown in Table 5:

Table 5: Average percentage of availability, utilization, and performance of shovel, truck, and dozer.

	Shovel	Truck	Dozer
Availability	74 (80)	56 (67)	35 (70)
Utilization	54 (58)	27 (50)	29 (45)
Performance	42	34	31

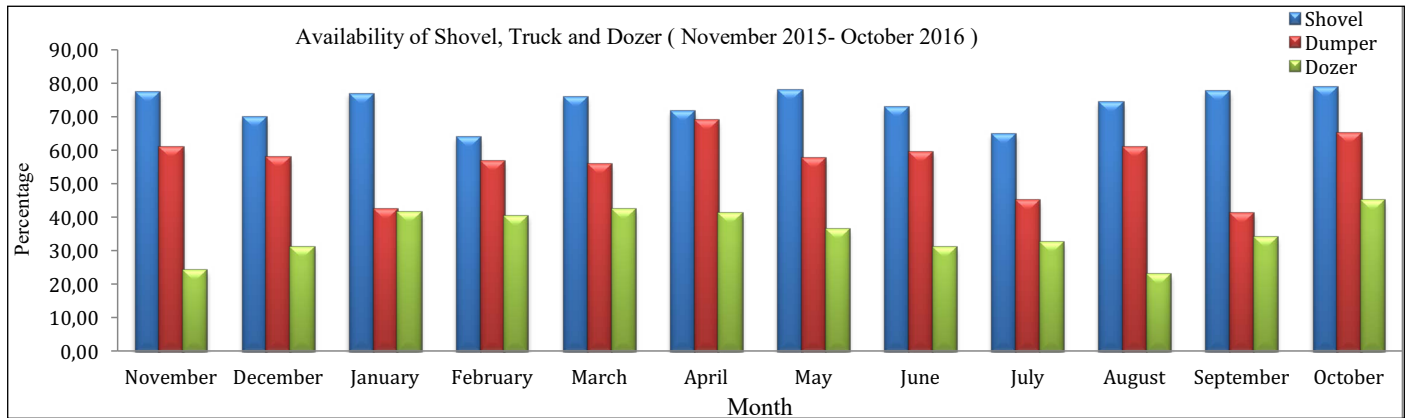


Figure 3. Availability of Shovel, Truck, and Dozer

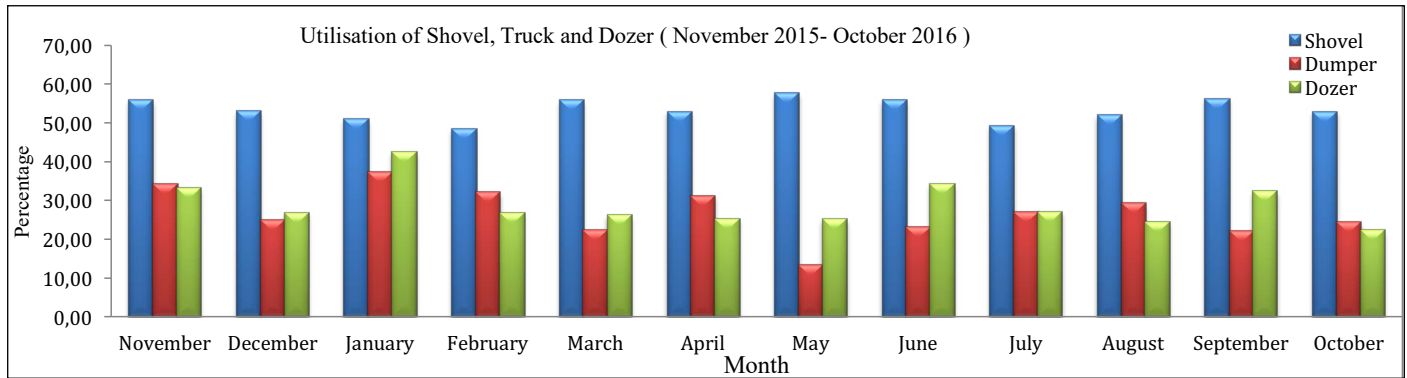


Figure 4. Utilisation of Shovel, Truck, and Dozer

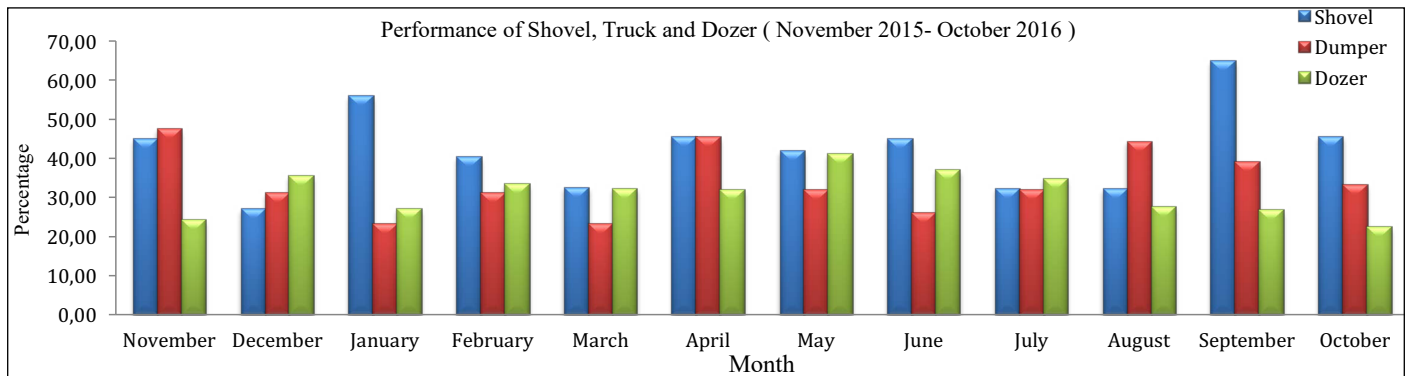


Figure 5. Performance of Shovel, Truck, and Dozer

Using the weights presented in Equations (19) - (21) the value of MPI for each machine is calculated using Equation (1) as follows:

$$MPI_{Shovel} = Av^{0.60} \times Ut^{0.05} \times Pp^{0.34} = 74^{0.60} \times 54^{0.05} \times 42^{0.34} = 57.55 \%$$

$$MPI_{Truck} = Av^{0.60} \times Ut^{0.04} \times Pp^{0.36} = 56^{0.60} \times 27^{0.04} \times 34^{0.36} = 45.45 \%$$

$$MPI_{Dozer} = Av^{0.54} \times Ut^{0.03} \times Pp^{0.43} = 35^{0.54} \times 29^{0.03} \times 31^{0.43} = 33.03 \%$$

4.3. Root Cause Analysis

Root cause analysis is best accomplished by a multidisciplinary cross-functional team of experts in different sectors as it would provide complementary skills (Guerin, 2015). In the study, data collection is done through personal observations, consensus building, and semi-structured interviews with a cross-functional team of 15 employees from different departments such as mining (excavation), electrical and mechanical engineering, safety, and personnel at the worksite and area office of the mine. The mine visits help to examine the physical environment and the usual work processes through direct interaction with the staff which is followed by reviews of relevant documentation and literature for formulating recommendations and actions. The semi-structured interview follows a deductive query technique in which a series of "why" and "caused by" questions were asked 3 or more times to identify the potential causes and various sub-clauses/factors that contributed to the potential causes. The query discontinues when no more causes can be attributed to the effect, hence here, the root causes are deduced. CED is done with suggestions from the literature (Papic et al., 2016; Sharma and Sharma, 2010; Ishikawa, 1990) which is adapted for the study. The ineffectiveness of the dozer is enumerated and visualized on the Ishikawa diagram

which is analyzed using the methodology proposed in Section 3. Hence, 5 root causes are identified based on 4 broad categories related to machine, material, manpower, and method as illustrated in Figure 6.

5. Discussions

The study explores the application of MPI and CED to examine the productivity of the fleet of 3 mining types of equipment through bottleneck identification and RCA. The study reveals that the dozer fleet is the bottleneck equipment. The effectiveness of the dozers may be improved with an increase in their performance. While the weight assessment suggests that utilization is the criteria that must be focused on strongly for improvement.

The study demonstrates to development of significant insights into the root causes of the ineffectiveness of dozers by exploring various failure factors. The finding from the RCA reveals a significant proportion of the causes are related to machine, material, manpower, and method. Several maintenance-related measures are proposed in the root cause analysis. The scheduling and planning of the dozer need to be checked for performance and productivity improvement. Maintenance outsourcing of the entire fleet of a dozer or some maintenance functions is one of the mitigation measures for maintenance managers and operators for the effectiveness of the dozer. Efficient maintenance can also be achieved by improved instructions on the maintenance of the dozer; continuous monitoring of the maintenance procedures such as cleaning or lubrication and appraisal of the inspection gap; and periodic inspection like minor servicing and repair, re-setting the machine to acceptable performance level and assessment of the quality of lubricants used.

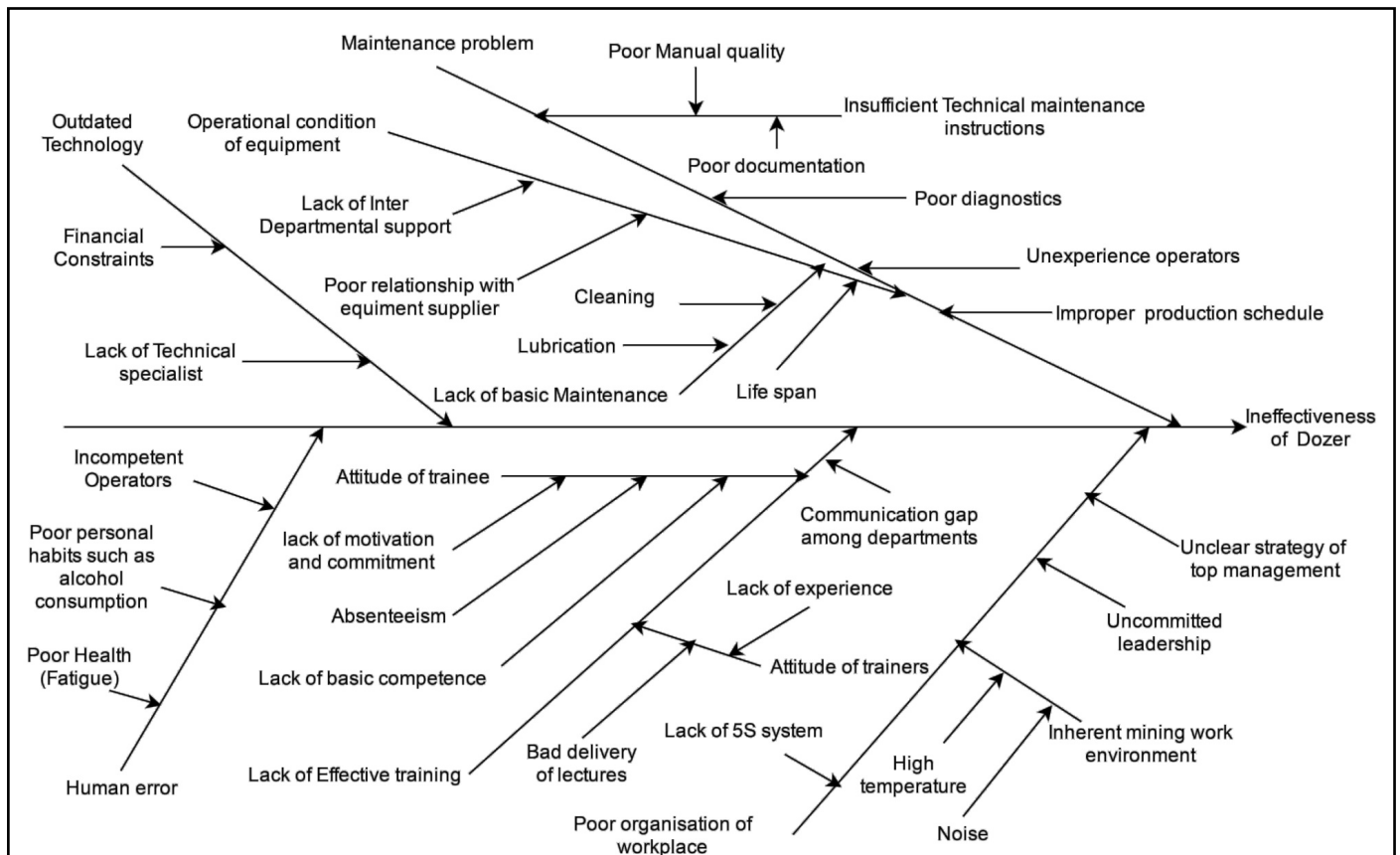


Figure 6. Cause and Effect Diagram for Ineffectiveness of Dozer

There is a significant need for the validation of theoretical knowledge and techno-managerial skills in the mine. Some of the mitigation measures for manpower-related causes such as lack of skill, working instructions, individual training and characteristics, and job experience would be personnel re-training; categorizing tasks based on complexity and assigning difficult task for more experienced personnel; developing task usage, inspection manuals and check-lists of equipment; educating operators about the importance of work standardization which helps in minimizing the consumption of resources; and augmenting employee motivation and commitment through participation in decision making.

Thus, exploring the root causes of the ineffectiveness of the dozers is important as it will avail the practitioners/employees with the opportunity of choosing and execute the maintenance strategies more effectively, thereby maximizing the equipment performance and productivity.

6. Conclusions

This study demonstrated a case analysis of a coal mine that can be applied for the productivity improvement of the Indian coal mining industry. In the study, the productivity of 3 mining equipment is analyzed using MPI. The study found that the dozers are the production bottleneck machine for the period of case analysis based on their MPI value. Thus, the dozers have less effectiveness for production as compared to the shovels and trucks. The result is validated with the secondary data from the mining department and personal management of the mine. The study reveals that not only productivity improvement but lean mining could be achieved by eliminating or reducing the inconsistency between the produced output and the desired output after bottleneck analysis. The improvement solutions and the mitigating measures are suggested based on the detected bottleneck and dominant factor through MPI comparison and evaluation using RCA. A CED was performed to eliminate the effect of bottleneck equipment. In this study, it has been observed that MPI and RCA can be implemented to improve the productivity of the equipment. The study identifies the root and contributory factors of the ineffectiveness of the dozer in the mine and suggests risk reduction strategies and the development of action plans to assess the effectiveness of the strategies.

The highly dynamic nature of the mining environment may constrain the evaluation of the process effectiveness using MPI thereby affecting the decision-making. The conclusion from the study is based on personal judgments of the experts and employees for the case mine which may limit the study to ensure external validity.

In RCA, the derived causal relations may not empirically link to the effect under examination owing to its predominantly expert dependence. Thus, semi-quantitative techniques such as Failure Mode and Effect Analysis (FMEA) can be employed in future studies. Moreover, the findings can be externally validated with multiple cases through real-world implementation or simulation.

References

- Aboumradi, M., Shiner, B., Riblet, N., Mills, P.D., Watts, B.V. 2018. Factors contributing to cancer-related suicide: A study of root-cause analysis reports. *Psycho-Oncology*. 27 (9), 2237-2244.
- Ahmed, M., Ahmad, N. 2011. An application of Pareto analysis and cause-and-effect diagram (CED) for minimizing rejection of raw materials in the lamp production process. *Management Science and Engineering* 5(3), 87.
- Andersen, B., Fagerhaug, T. 2006. *Root cause analysis: simplified tools and techniques*, ASQ Quality Press.
- Arputharaj, M. M. 2015. Studies on availability and utilization of mining equipment-an overview. *International Journal of Advanced Research in Engineering and Technology*. 6 (3), 14-21.
- Ayag Z., Gurcan Ozdemir, R. 2012. Evaluating machine tool alternatives through modified TOPSIS and alpha-cut based fuzzy ANP. *International Journal of Production Economics*. 140(2), 630-636.
- Belhadi, A., Touriki, F.E., Fezazi, S.E. 2017. Prioritizing the solutions of lean implementation in SMEs to overcome its barriers: An integrated fuzzy AHP-TOPSIS approach. *Journal of Manufacturing Technology Management*. 28 (8), 1115-1139.
- Beikkhakhian, Y., Javanmardi, M., Karbasian, M., Khayambashi, B. 2015. The application of ISM model in evaluating agile supplier's selection criteria and ranking suppliers using fuzzy TOPSIS-AHP methods. *Expert Systems with Applications*. 42 (15), 6224-6236.
- Buckley, J.J., Qu, Y. 1990. On using alpha-cuts to evaluate fuzzy functions. *Fuzzy Sets System*, 38, 309-312.
- Chang, D.Y. 1996. Applications of the extent analysis method on fuzzy AHP. *European Journal of Operational Research*. 95 (3), 649-655.
- Cheng, C. H. 1999. Evaluating weapon systems using ranking fuzzy numbers. *Fuzzy Sets and Systems*. 107(1), 25-35.
- Duggett, A. M. 2004. A Statistical Comparison of Three Root Cause Tools. *Journal of Industrial Technology*. 20 (2), 1-9.
- Elevli, S., Elevli, B. 2010. Performance measurement of mining equipment by utilizing OEE. *Acta Montanistica Slovaca*. 15(2), 95-101.
- Farhan, U.H., Tolouei-Rad, M., Osseiran, A. 2016. Use of AHP in decision-making for machine tool configurations. *Journal of Manufacturing Technology Management*. 27(6), 874-888.
- Guerin, T. 2015. An investigation into the cause of loss of containment from the supply of mini-bulk lubricants. *Engineering Failure Analysis*. 54, 1-12.
- Huang, Y.P., Basanta, H., Kuo, H.C., Huang, A. 2018. Health symptom checking system for elderly people using fuzzy analytic hierarchy process. *Applied System Innovation*, 1(2), 10.
- Ishikawa, K. 1990. *Introduction to quality control*, Productivity Press.
- Kang, H.Y., Lee, A.H.I., Yang, C.Y. 2012. A fuzzy ANP model for supplier selection as applied to IC packaging. *Journal of Intelligent Manufacturing*, 23 (5), 1477-1488.
- Kamaruzzaman, S.N., Lou, E.C.W., Wong, P.F., Wood, R., Che-Ani, A.I. 2018. Developing weighting system for refurbishment building assessment scheme in Malaysia through analytic hierarchy process (AHP) approach. *Energy Policy*. 112, 280-290.
- Kellogg, K.M., Hettinger, Z., Shah, M., Wears, R.L., Sellers, C.R., Squires, M. and Fairbanks, R.J. 2017. Our current approach to root cause analysis: is it contributing to our failure to improve patient safety. *BMJ Quality Safety*. 26 (5), 381-387.
- Kesimal, A., Bascetin A. 2002. Application of Fuzzy Multiple Attribute Decision Making in Mining Operations. *Mineral Resources Engineering*. 11(1), 59-72.
- Khaba, S., Bhar, C. 2017. Quantifying SWOT analysis for the Indian coal mining industry using Fuzzy DEMATEL. *Benchmarking: An International Journal*. 24(4), 882-902.
- Kim, J., Lee, J., Kim, B., Kim, J. 2019. Raw material criticality assessment with weighted indicators: An application of fuzzy analytic hierarchy process. *Resources Policy*. 60, 225-233.
- Kutlu, A.C., Ekmekçioğlu, M. 2012. Fuzzy failure modes and effects analysis by using fuzzy TOPSIS-based fuzzy AHP. *Expert Systems with Applications*, 39 (1), 61-67.
- Lanke, A. A., Hoseinie, S. H., Ghodrati, B. 2016. Mine production index (MPI)-extension of OEE for bottleneck detection in mining. *International Journal of Mining Science and Technology*. 26 (5), 753-760.

- Lanke, A., Hoseinie, H., Ghodrati, B. 2014. Mine production index (MPi): new method to evaluate the effectiveness of mining machinery. In International conference on mining and mineral engineering (ICMME 2014), 755-759.
- Lee, A., Lin, C.Y., Wang, S. R., Tu, Y. M. 2010. The construction of a comprehensive model for production strategy evaluation. *Fuzzy Optimization and Decision Making*, 9(2), 187-217.
- Lee, T. R., Thi P. H. L., Andrea G., Lenny S. C. K. 2011. Using FAHP to determine the criteria for partner's selection within a green supply chain: The case of hand tool industry in Taiwan. *Journal of Manufacturing Technology Management*, 23 (1), 25-55.
- Lundberg, A., Dangel, R.F. 2019. Using root cause analysis and occupational safety research to prevent child sexual abuse in schools. *Journal of child sexual Abuse*, 28(2), 187-199.
- Mowafi, Y.A., Alaqarbeh, T., Alazrai, R. 2019. Putting Context in the Network Access of Mobile Applications Using Fuzzy Analytic Hierarchy Process. *International Journal of Decision Support System Technology*. 11 (2), 13-26.
- Nazari, S., Fallah, M., Kazemipoor, H., Salehipour, A. 2018. A fuzzy inference-fuzzy analytic hierarchy process-based clinical decision support system for diagnosis of heart diseases. *Expert Systems with Applications*. 95, 261-271.
- Papic, L., Kovacevic, S., Galar, D., Thaduri, A. 2016. Investigation of Causes of Mining Machines Maintenance Problems, *Current Trends in Reliability, Availability, Maintainability and Safety*. 283-299, Springer.
- Prakash, C., Barua, M. K., Pandya, K. V. 2015. Barriers analysis for reverse logistics implementation in Indian electronics industry using fuzzy analytic hierarchy process. *Procedia-Social and Behavioral Sciences*. 189, 91-102.
- Pendred, S., Fischer, A., Fischer, S. 2016. Improved management effectiveness of a marine protected area through prioritizing performance indicators. *Coastal Management*. 44 (2), 93-115.
- Reid, I., Smyth-Renshaw, J. 2012. Exploring the fundamentals of root cause analysis: are we asking the right questions in defining the problem. *Quality and Reliability Engineering International*. 28 (5), 535-545.
- Saaty, T. L. 1980. *The Analytic Hierarchy Process*. New York: McGraw Hill.
- Sharma, R. K., Sharma, P. 2010. System failure behavior and maintenance decision-making using, RCA, FMEA, and FM. *Journal of Quality in Maintenance Engineering*. 16, 64-88.
- Shaw, K., Shankar, R., Yadav, S. S., Thakur, L. S. 2012. Supplier selection using fuzzy AHP and fuzzy multi-objective linear programming for developing a low-carbon supply chain. *Expert systems with applications*. 39 (9), 8182-8192.
- Wilson, P. F., Dell, L. D., Anderson, G. F. 1993. *Root Cause Analysis: A Tool for Total Quality Management*. ASQC Quality Press.
- Yu, M.C., Goh, M., Lin, H. C. 2012. Fuzzy multi-objective vendor selection under lean procurement. *European Journal of Operational Research*, 219 (2), 305-311.
- Zadeh, L. A. 1965. Fuzzy sets. *Information and Control*, 8(3), 338-353.
- Zyoud, S.H., Kaufmann, L.G., Shaheen, H., Samhan, S., Fuchs-Hanusch, D. 2016. A framework for water loss management in developing countries under fuzzy environment: Integration of Fuzzy AHP with Fuzzy TOPSIS. *Expert Systems with Applications*. 61, 86-105.



Original Research

Multi-Factor Optimization of Adjacent Layered Salt Rock Storage Based on Response Surface Methodology

Jinyi Ji^{a,*}, Baokun Zhou^{b,**}, Zhichen Tao^{c,***}, Xiaoqing Chen^{a,****}

^a School of Mining Engineering, University of Science and Technology Liaoning, Anshan 114051, China

^b School of Energy and Mining, China University of Mining and Technology (Beijing), Beijing 100083, China

^c Anshan Iron and Steel Group Corporation, Anshan 114001, China

Received: 18 November 2022 • Accepted: 24 July 2023

ABSTRACT

In order to improve the utilization efficiency of salt rock mines when storing natural gas, it is necessary to clarify the influence of different factors on adjacent underground laminated salt rock caverns. In view of this, 15 groups of simulation tests are designed by using the Response Surface Methodology (RSM). A quadratic response surface model with the midpoint displacement and cavern waist stress of the interlayer as the response values is constructed. The influence of the interaction between pillar width, interlayer thickness and the location of a single interlayer on the midpoint displacement of the interlayer and the internal waist stress of the adjacent ellipsoidal cavity is studied. The results show that the interlayer thickness is the main influence factor of the midpoint displacement of the interlayer, and the pillar width is the main influence factor of the cavern waist stress. When the adjacent storage is designed as a pillar width of 2.5D, an interlayer thickness of 2 m, and the midpoint of the interlayer is 0.3H above the cavity, the displacement and stress of the test model are relatively small. The results can provide a certain reference for the mechanical analysis of adjacent underground layered salt rock gas storage.

Keywords: layered salt rock gas storage, multi-factor optimization, response surface methodology, finite element simulation, main influence factor

Introduction

Salt rock is an ideal oil and gas storage medium for oil and gas storage due to its low permeability and optimal creep property (Liu et al., 2016; Wanyan et al., 2019; Bakhtiari et al., 2021). Compared with the aboveground storage methods, salt rock storage has the advantages of flexible injection and production, large single-well throughput, and a high proportion of working gas (Yang, 2017; Liu et al., 2018). In addition, underground salt rock also has the characteristics of safety, saving land resources, capital and environmental protection, which is an effective way to ensure energy security (Zivar et al., 2021; Liu et al., 2020; Shad et al., 2022). The history of underground gas storage in salt rock in some countries is earlier, and the designed operation life of gas storage has been up to 80 or even hundreds of years (Patroni, 2007). China's natural gas business is developing rapidly, but the lack of gas storage capacity is still a bottleneck restricting its sustainable and high-quality development. To solve this problem, a master plan has been set to speed up the construction of underground stor-

age facilities. It will take five years to complete the total new peak capacity in the first 20 years (National Energy Administration, 2022). It is estimated that the future natural gas production will continue to grow for a long time (Lu et al., 2018). Increasing the construction of gas storage is of great significance for easing the tension between gas supply and demand in China and promoting the rapid development of economy.

To study the stability in underground salt rock storages, a geomechanical model test of Jintan underground salt rock storages was carried out to obtain the creep deformation and stress distribution of surrounding rock during the operation of gas storage (Dai et al., 2009). Jing et al. (2012) summarized the 7 factors that may affect the shrinkage deformation of salt rock storage. They presented that the operation mode of two adjacent gas storage caves (adjacent caverns or adjacent cavities for short), the ratio of low-pressure operation time in a single cycle, and the ratio of cavity height to the diameter are the main sensitive factors. Jia et al. (2014) studied the influence of geometric distribution form of el-

**** Corresponding author: xiaogchen012@126.com • <https://orcid.org/0000-0001-6714-1631>

* jild0961@163.com • <https://orcid.org/0000-0002-9277-6206>

** zhouling830@126.com • <https://orcid.org/0000-0003-0754-9226>

*** liujiangtao012@sina.com • <https://orcid.org/0000-0002-1812-2685>

lipsoidal cavity, pillar width and interlayer position on the stability of gas cavern by orthogonal experiments. Since it was proved that the interlayer position was the most significant influencing factor, the interaction between different factors and parameters cannot be effectively reflected.

Taking the underground salt rock storage in Jintan, China as the test background, reasonable test factors are selected by referring to the test parameter settings in some articles and engineering practices. 15 test plans are established by the response surface method, and the test data are obtained by establishing corresponding test models with the professional finite element simulation software. The effects of the pillar width, interlayer thickness and interlayer position on adjacent gas storage chambers are studied. Through the main effect analysis and response surface analysis of the test results, the significance and optimum level of each factor are obtained, and the optimum form of adjacent caverns during the construction of salt rock storage groups is established.

1. Parameter design of adjacent storage

The Jintan salt rock layer in Jiangsu Province is located about 1000 m deep underground with a thickness of 67.85 m to 230.95 m. The interlayer of salt rock has two layers with an average thickness of 3.02 m and 2.50 m. As of March 2023, 99 underground caverns of salt rock have been built or under construction in this salt mining area, with a single salt cavern volume of about 200,000-300,000 m³, a cavern diameter of about 70 m, a height of about 150 m, and a design pressure of about 17 MPa (Jiangsu provincial department of natural resources, 2021). The rock physical and mechanical parameters of the salt mine area are shown in Table 1 (Zhang et al., 2009). The test will use the above parameters as the basis for the gradient design of the experimental data.

Table 1: Basic parameters of strata

Formation	Elasticity modulus /GPa	Poisson ratio	Density / (kg/m ³)	Cohesion /MPa	Internal friction angle / (°)
Mudstone	10	0.27	2350	1.0	35
Interlayer	4	0.30	2350	0.5	30
Salt rock	18	0.30	2200	1.0	45

This test mainly studies the influence of different factors on the displacement and stress of sensitive parts of adjacent chambers. When simulating the initial stress of rock mass, only the gravity of rock layer is considered in the test, and Drucker-Prager model is used for numerical calculation. When simulating the initial stress of rock mass, only the static analysis of rock mass gravity is considered and the Drucker-Prager model is selected for numerical calculation. To study the influence of different factors on the stress and displacement at sensitive positions of adjacent cavities, 15 groups of corresponding three-dimensional numerical models are established to simulate the stress and displacement of adjacent cavities using the professional finite element simulation software after determining the research scheme. The calculation area is set as a cube of 800 m *800 m *400 m, and the weight of the overlying strata 700 m above the cube is simplified to the load on the top surface of the model. Based on the thickness of overburden rock and the average density of mudstone, the equivalent load above the cube is about 16 MPa. Four vertical surfaces are constrained by normal directions perpendicular to the surface. According to the actual situation of the project, the long axis of the storage cham-

ber is 150 m and its short axis is 70 m. For different test schemes, pillar width, interlayer thickness and interlayer position will vary. Figure 1 shows the cross section of the storage model with a pillar width of 105 m, an interlayer thickness of 3 m, and the interlayer midpoint is 75 m below the top of the cavern.

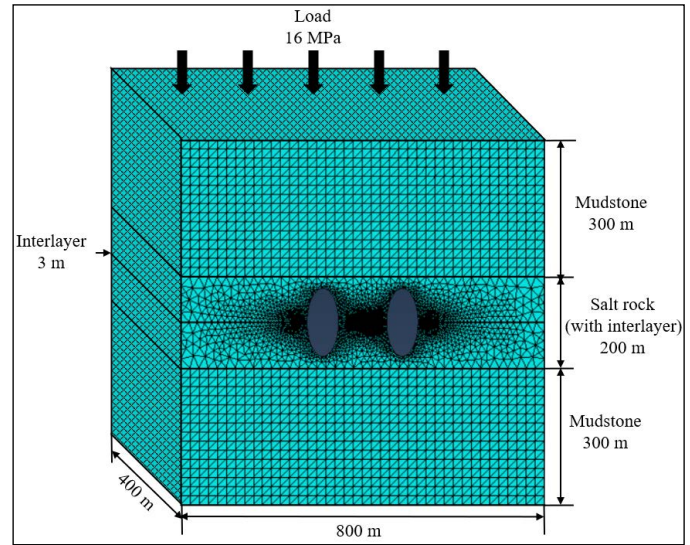


Figure 1. Cross section of the adjacent gas storage model

1.1 Design of pillar width

The overall stability of the gas storage group is closely related to the pillar width. Too narrow pillars may lead to instability and destruction of the gas storage chamber, and too wide pillars may reduce the utilization rate of salt rock mines. To prevent the destruction of gas cavern and improve the utilization efficiency of salt rock mines, a reasonable pillar width is necessary. Through the simulation of the rheology geology of the storage group with similar materials from a salt rock reservoir media model, Zhang et al. (2012) concluded that the pillar width should be greater than 1.5 times the maximum diameter of the chamber. Wang et al. (2011) used FLAC3D to establish a finite element calculation model for the simulation of saltrock gas caves. It is suggested that the width of pillars between two adjacent salt rock caves should be 2-3 times the diameter of salt cavern. Liu et al. (2011) and Jia et al. (2014) obtained an optimum pillar width 2 times the diameter of salt cave by different experimental design methods. Taking into account the above results, and to avoid waste of salt area caused by too wide pillars, the pillar width is designed to be 105 m, 140 m and 175 m, i.e. 1.5D (diameter), 2.0D and 2.5D respectively. D is the maximum diameter of the cavity waist, and 1D=70 m, as shown in Figure 2.

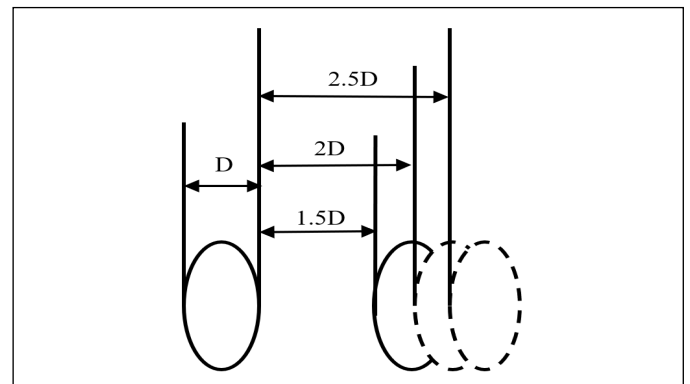


Figure 2. Design of pillar width

1.2 Design of interlayer thickness

The existence of an interlayer in a layered salt rock has an important impact on the stability of surrounding rock. Many studies show that the interlayer is usually a part of layered salt rocks prone to deformation (National Energy Administration, 2022; Lu et al., 2018). According to a creep fatigue-failure model of salt rock, Moghadam et al. (2015) found that the stability of caverns was significantly affected when the cavern surface contacted the interlayer. According to an average thickness of interlayers in a salt rock (Jiangsu provincial department of natural resources, 2021), the interlayer thickness is set as 2 m, 3 m and 4 m respectively.

1.3 Design of cavity interlayer position

According to Lu et al. (2018), the interlayer position has little influence on the stability of storage group. Jia et al. (2014) believed that there was a gap in the stress level due to different positions of the interlayer relative to the cavity. The stress level of the interlayer controls the stability of the interlayer, and then affects the stability of the cavity. It is believed that the interlayer position has a great impact on the stability of caverns. According to the results of Jia et al. (2014) and Zhang et al. (2022), the positions of the test interlayer are set as 45 m, 75 m and 105 m, i.e. $0.3H$ (height), $0.5H$ and $0.7H$ respectively. H is the maximum height of the cavity, indicating the distance between the midpoint of the interlayer and the top of the cavity in the vertical direction, and $1H=150$ m, as shown in Figure 3.

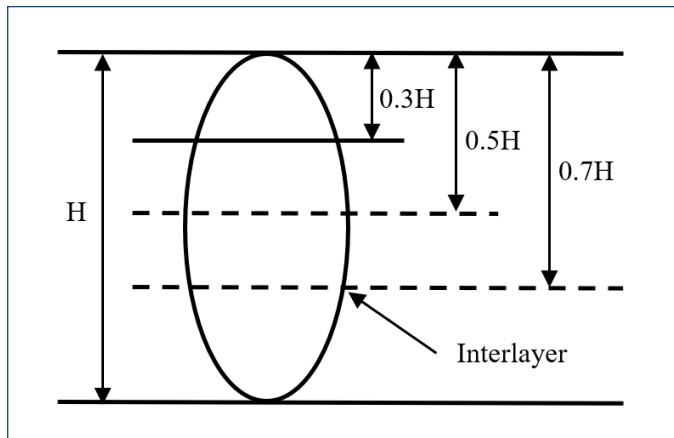


Figure 3. Design of interlayer position

2. Response surface test

2.1 Design of test scheme

Response Surface Methodology (RSM) is a statistics-based optimization method that combines the experimental design and mathematical model. It can be used to explore the mathematical relationship between multiple influencing factors and response output (Zhou et al., 2021). In this study, RSM is used to explore the influence of pillar width, interlayer thickness, interlayer position, and their interaction on the stability of adjacent cavities in the design of adjacent storages of layered salt rocks. The optimal design effect was obtained through different design tests (Chen et al., 2017). Box-Behnken Design (BBD) method was used to design the 3-factor experiment, as shown in Table 2. The code values are randomly generated by the professional data analysis software.

Table 2. Scheme design of response surface of the test factor

Test number	Code value	Pillar width(A)/m	Interlayer thickness (B)/m	Interlayer position (C)/m
1	A ₁ B ₂ C ₃	105	3	105
2	A ₁ B ₁ C ₂	105	2	75
3	A ₂ B ₂ C ₂	140	3	75
4	A ₃ B ₃ C ₂	175	4	75
5	A ₁ B ₃ C ₂	105	4	75
6	A ₂ B ₃ C ₃	140	4	105
7	A ₂ B ₃ C ₁	140	4	45
8	A ₂ B ₂ C ₂	140	3	75
9	A ₃ B ₁ C ₂	175	2	75
10	A ₃ B ₂ C ₃	175	3	105
11	A ₂ B ₁ C ₃	140	2	105
12	A ₂ B ₂ C ₂	140	3	75
13	A ₁ B ₂ C ₁	105	3	45
14	A ₃ B ₂ C ₁	175	3	45
15	A ₂ B ₁ C ₁	140	2	45

2.2 Test results and model analysis

According to the experimental scheme designed in Table 2, the corresponding finite element numerical simulation model is established, and the stress and deformation displacement of different parts of adjacent caverns are obtained when the model is loaded. As shown in Table 3, the result data of 15 groups of experiments designed by BBD and the corresponding models includes the horizontal displacement of the cavern waist and the midpoint of pillar interlayer (denoted as S and T), the equivalent stress at the midpoint of the cavern waist and the pillar interlayer (denoted as V and W), and the equivalent stress at the midpoint of the pillar and the interlayer (denoted as Y and Z). The response surface calculation function in the data analysis software is used to analyze the response surface of 6 groups of data in Table 3, and the fitting degree of different models in Table 4 is summarized. The fitting distance is measured in response variables, which represents the distance between the data value and the fitted value. The lower the fitting distance value, the higher the degree of response described by the model. The higher the R-sq (R^2) value, the higher the fitting degree between the model and the data. R-sq is always between 0% and 100%. R-sq (forecast) can be used to determine the degree to which the model can predict the response to new observations, and the model with larger R-sq (forecast) values also has better prediction.

In the correlation coefficient of the response surface function fitting of the model, the prediction R-sq by the response surface regression model for the midpoint displacement of the interlayer, the cavern waist stress, and the pillar central stress is more than 90%. It shows that the predicted data of the response surface model function is consistent with the actual data, and the error is small. It can be used to analyze and predict the effect of parameters set in the test on the adjacent caverns. Through the response results of pillar central stress, it is strongly influenced by the pillar width and can be classified as linear correlation, and is not the focus of this test. The prediction R-sq of the response surface regression model of other parameters cannot reach 90%, and no further analysis will be made.

Table 3. Regression test results of different response values

Test number	S/mm	T/mm	V/MPa	W/MPa	Y/MPa	Z/MPa
1	14.36	14.57	29.83	25.34	21.49	19.97
2	14.72	15.54	30.00	26.24	21.45	20.82
3	15.39	16.82	29.17	25.15	19.02	18.71
4	15.60	17.79	28.93	24.59	17.53	17.39
5	15.54	17.85	30.34	25.77	21.49	20.89
6	15.04	15.84	29.03	24.51	19.10	18.29
7	15.10	15.98	29.01	24.47	19.15	18.32
8	15.39	16.82	29.17	25.15	19.02	18.71
9	15.12	15.82	28.73	25.06	17.48	17.32
10	15.14	15.02	28.35	24.49	17.59	17.12
11	14.76	13.93	28.56	25.18	19.03	18.23
12	15.39	16.82	29.17	25.15	19.02	18.71
13	14.37	14.67	29.84	25.32	21.49	20.00
14	15.13	15.18	28.31	24.43	17.59	17.14
15	14.75	14.06	28.57	25.14	19.03	18.24

Table 4. Fitting degree of test models with different response values

Model summary	Fitting distance	R-sq	R-sq(ad-justment)	R-sq(forecast)
S and ABC	0.2011109	90.52%	73.45%	0.00%
T and ABC	0.136949	99.57%	98.79%	93.08%
V and ABC	0.0784538	99.43%	98.39%	90.82%
W and ABC	0.116662	98.15%	94.82%	70.42%
Y and ABC	0.0271109	99.99%	99.97%	99.81%
Z and ABC	0.203973	99.05%	97.37%	84.78%

Multivariate nonlinear quadratic fitting is performed on the interlayer midpoint displacement (*T*) and cavern waist stress (*V*) in Table 3, and the regression equations expressed in uncoded units areas (1) and (2):

$$T = -0.78 + 0.0311A + 1.293B + 0.3132C - 0.000066A^2 + 0.0112B^2 - 0.002088C^2 - 0.00243AB - 0.000014AC - 0.00008BC \quad (1)$$

$$V = 33.88 - 0.0891A + 0.183B + 0.064C + 0.000253A^2 + 0.02B^2 - 0.000442C^2 - 0.001AB + 0.000012AC + 0.00025BC \quad (2)$$

F-value and P-value are used to analyze the significance of each coefficient in the above equation. The results are shown in Table 5 and Table 6. F-value analysis is also called F-test or ANOVA (analysis of variance), which is used to evaluate the differences between groups. F-value represents the significance of the whole fitting equation. The larger the F-value, the more significant the equation and the better the fitting degree. P-value is a parameter used to determine the results of hypothesis test, which reflects the regression effect of parameters. The smaller the P-value, and the more

significant the results (Zhou et al., 2021). In addition, whether the test result is “insignificant”, “significant” or “highly significant” needs to be determined by the P-value and the actual problems. In this experiment, $P \geq 0.05$ means that the regression effect of this factor is not significant; $0.001 \leq P < 0.05$ means that the regression effect of this factor is generally significant, and $P < 0.001$ means that the regression effect of this factor is highly significant.

Table 5. Response surface regression model of interlayer midpoint displacement

Source	DoF	Adj-SS	Adj-MS	F-value	P-value	Significant
Model	9	21.5935	2.3993	127.93	<0.001	Highly significant
A	1	0.174	0.174	9.28	0.029	Significant
B	1	8.2215	8.2215	438.36	<0.001	Highly significant
C	1	0.0351	0.0351	1.87	0.23	Insignificant
AA	1	0.0244	0.0244	1.3	0.306	Insignificant
BB	1	0.0005	0.0005	0.02	0.881	Insignificant
CC	1	13.0327	13.0327	694.89	<0.001	Highly significant
AB	1	0.0289	0.0289	1.54	0.27	Insignificant
AC	1	0.0009	0.0009	0.05	0.835	Insignificant
BC	1	0	0	0	0.972	Insignificant
Error	5	0.0938	0.0188			
Loss	3	0.0938	0.0313			
Pure error	2	0	0			
Total	14	21.6873				

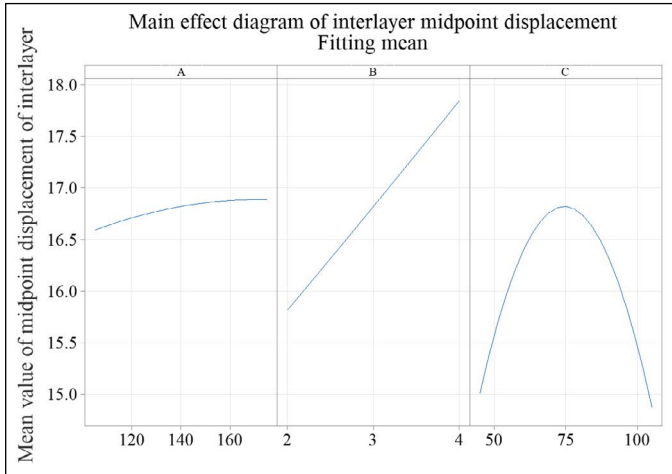
Table 6. Response surface regression model of cavern waist stress

Source	DoF	Adj-SS	Adj-MS	F-value	P-value	Significant
Model	9	5.33258	0.59251	96.26	<0.001	Highly significant
A	1	4.04701	4.04701	657.52	<0.001	Highly significant
B	1	0.26281	0.26281	42.7	0.001	Significant
C	1	0.0002	0.0002	0.03	0.864	Insignificant
AA	1	0.35483	0.35483	57.65	0.001	Significant
BB	1	0.00148	0.00148	0.24	0.645	Insignificant
CC	1	0.58341	0.58341	94.79	<0.001	Highly significant
AB	1	0.0049	0.0049	0.8	0.413	Insignificant
AC	1	0.00063	0.00063	0.1	0.763	Insignificant
BC	1	0.00023	0.00023	0.04	0.856	Insignificant
Error	5	0.03078	0.00616			
Loss	3	0.03078	0.01026			
Pure error	2	0	0			
Total	14	5.36336				

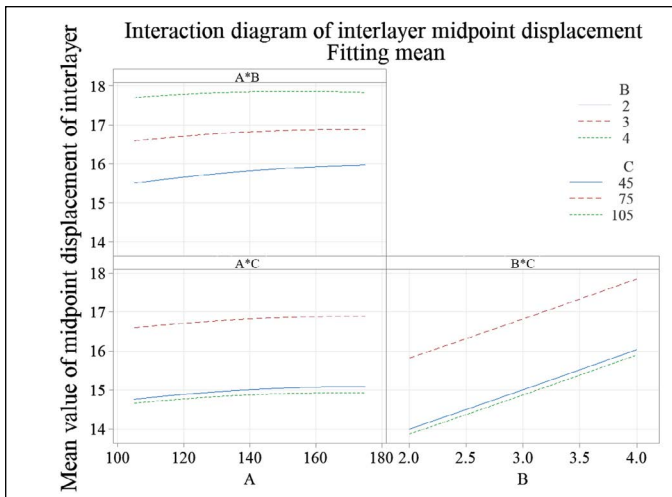
According to Table 5 and Table 6, the P-value of the interlayer midpoint displacement and the cavern waist stress response surface model are both less than 0.001, indicating that these two models are highly significant in fitting. In this model, the P-value of pillar width and interlayer thickness are both less than 0.05, indicating that they have significant effects on the midpoint displacement of the interlayer. The interlayer thickness has a highly significant effect on the midpoint displacement of interlayer, and the pillar width has a highly significant effect on the cavern waist stress.

2.3 Factor effect and response surface analysis

Based on the response surface prediction equation, the factor response diagram and response surface of the interaction between the midpoint displacement and cavern waist stress of the interlayer and the three influencing factors of the pillar width, interlayer thickness and interlayer position are shown in Figs. 4-7. The relationship between each factor and the response value can be seen intuitively in the factor response graph. In the response surface graph, the influence of the factor on the response value is reflected in the slope of the response surface. If the slope is steep, the influence of the factor is great; otherwise, it is small.

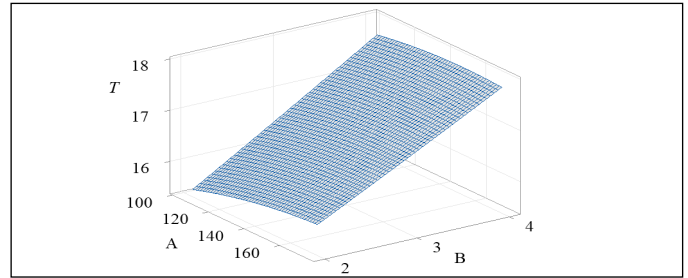


(a) Main effect diagram of interlayer midpoint displacement

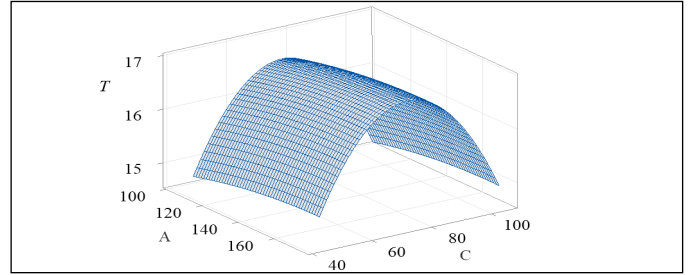


(b) Interaction diagram of interlayer midpoint displacement

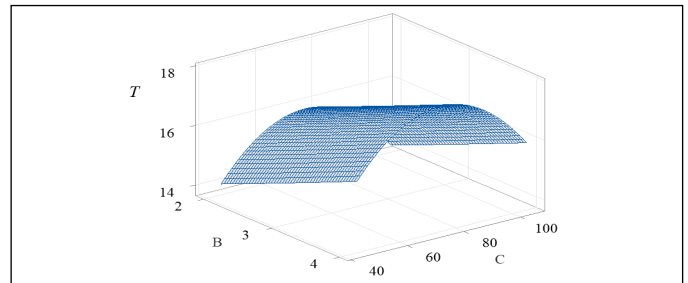
Figure 4. Factor response of interlayer midpoint displacement



(a) Effect of A*B

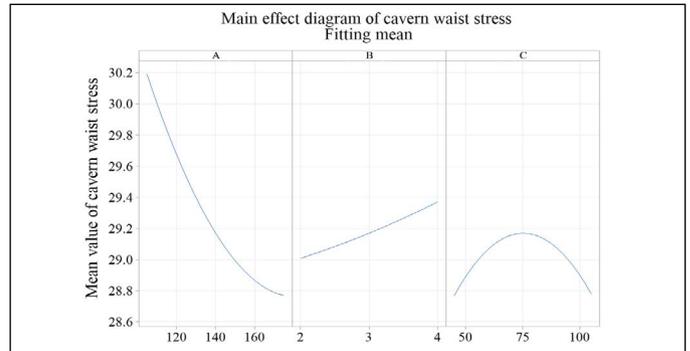


(b) Effect of A*C

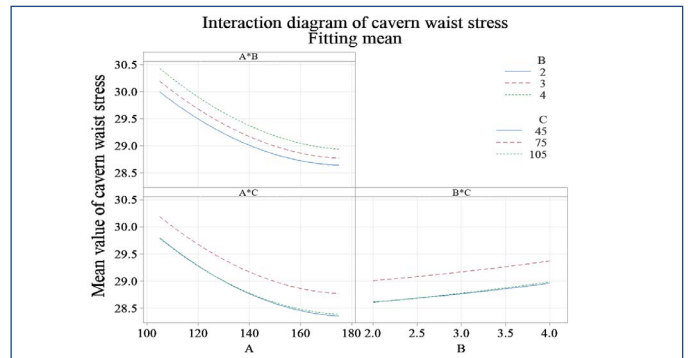


(c) Effect of B*C

Figure 5. Response surface of interlayer midpoint displacement

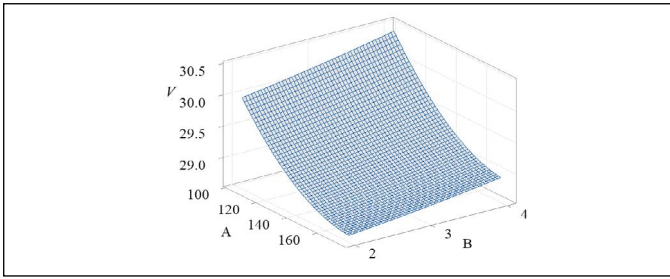


(a) Main effect diagram of cavern waist stress

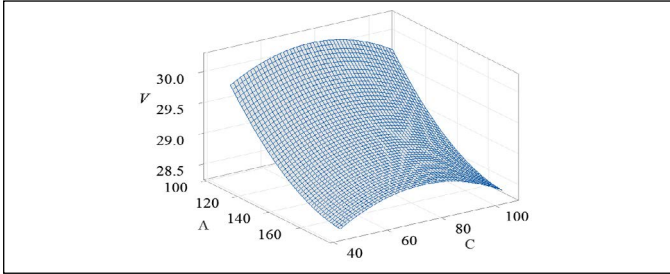


(b) Interaction diagram of cavern waist stress

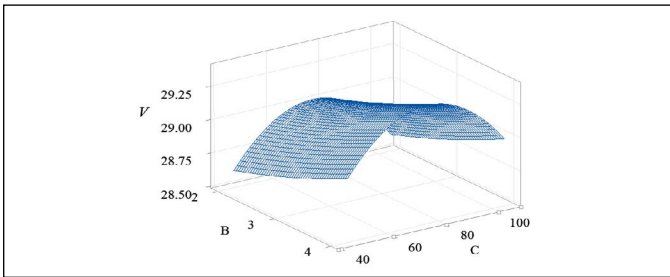
Figure 6. Factor response of cavern waist stress



(a) Effect of A*B



(b) Effect of A*C



(c) Effect of B*C

Figure 7. Response surface of cavern waist stress

It can be seen from Figure 4 and Figure 5 that the interlayer midpoint displacement increases slightly with the increase of the pillar width set in the test. Combined with the P-value of the interlayer thickness in Table 5, the displacement is mainly affected by the interlayer thickness and increases as it increases. When the interlayer is located at the waist of the cavity, the interlayer midpoint displacement is the largest and grows significantly with the increase of pillar width and interlayer thickness. It can be seen from Figure 5 (a) that the response surface is relatively steep. A and B have obvious interaction, and the displacement is more affected by the pillar width than the interlayer thickness. The optimal result is 105 m pillar width and 2 m interlayer thickness. It can be seen from Figure 5 (b) that the displacement first increases and then decreases as the interlayer depth increases, and the optimal result response is 105 m below the storage top. In Figure 5 (c), although the slope of the response surface is gentle, the range of displacement values is the largest. When the interlayer is located at the waist of the cavity, the displacement increases with the increase of the interlayer thickness.

Table 7. Multiple model response results

Response	Aim	Lower limit	Upper limit	Fitting value	SD of fitting value	Confidence interval 95%	Forecast interval 95%
S and ABC	Min	14.36	15.6	14.836	0.238	(14.225, 15.447)	(14.036, 15.636)
T and ABC	Min	13.93	17.85	14.169	0.162	(13.753, 14.585)	(13.624, 14.714)
V and ABC	Min	28.31	30.34	28.235	0.0927	(27.9967, 28.4733)	(27.9228, 28.5472)
W and ABC	Min	24.43	26.24	24.735	0.138	(24.381, 25.089)	(24.271, 25.199)
Y and ABC	Min	17.48	21.49	17.5325	0.032	(17.4502, 17.6148)	(17.4246, 17.6404)
Z and ABC	Min	17.12	20.89	16.991	0.241	(16.372, 17.611)	(16.180, 17.803)

It can be seen from Figure 6 and Figure 7 that the cavern waist stress decreases significantly with the increase of the pillar width set in the test. Based on the P-value of the pillar width in Table 6, the stress is mainly affected by the pillar width and increases with the decrease of the pillar width. When the interlayer is located at the waist of the cavity, the stress in the cavern waist is the largest and grows significantly with the increase of the interlayer thickness. It can be seen from Figure 7 (a) that the response surface is relatively steep, A and B have obvious interaction, and the stress is less affected by the interlayer thickness than the pillar width. The optimal results are 175 m pillar width and 2 m interlayer thickness. It can be seen from Figure 7 (b) that the stress first increases and then decreases with the increase of the interlayer depth, and the optimal result response is 45 m below the top of the storage. It can be seen from Figure 7 (c) that when the interlayer is located at the waist of the cavity, the stress increases with the increase of the interlayer thickness.

To determine the optimal form of adjacent caverns, 6 responses are required at least to obtain the optimal solution. In the data analysis software, the weights of 6 groups of response models are set to 1 for response, and the response results of multiple models are obtained as shown in Table 7. The optimal solution of the pillar width, interlayer thickness, and interlayer location is 175 m, 2 m and 45 m, respectively. As shown in Figure 8, a finite element model is built by the optimal solution, and the displacement and stress data at each location are obtained. The values of S, T, V, W, Y and Z are 14.92, 14.24, 28.13, 24.6, 17.54 and 17.10, respectively. Comparing the data with the fitted values and confidence intervals of the corresponding models in Table 7, it can be seen that the optimal solution model values are located in 95% confidence intervals and 95% prediction intervals. This shows that the predicted results of the multi-model response are consistent with the data obtained from the finite element model, and the error is small. To this end, the optimal solution model can be used to analyze and predict the influence of pillar width, interlayer thickness and interlayer position on the corresponding displacement and stress of adjacent caverns in Jintan.

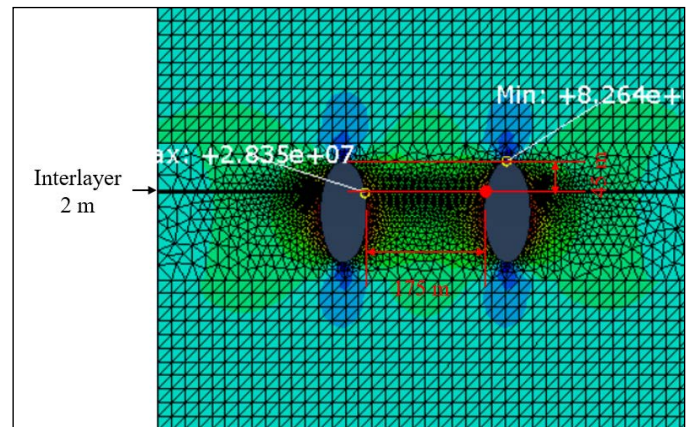


Figure 8. Finite element model of the optimal solution for each part

3. Conclusion

15 groups of simulation tests are designed using the Box-Behnken method of response surface model. The response surface model is established with the displacement of interlayer midpoint and the stress of the cavern waist as the response values. The thickness of the interlayer is the most significant factor of interlayer midpoint displacement, and the position of the interlayer follows the second. Pillar width is the most significant factor affecting the cavern waist stress, and the interlayer thickness and interlayer position are the subsignificant factors. According to the parameters set in the test, the optimal form of the adjacent storage is a pillar width of $2.5D$, an interlayer thickness of 2 m, and the midpoint of the interlayer is $0.3H$ above the cavity. Considering the stability and economy of the salt rock underground reservoir group, the column width can also be designed according to 2D.

The above static analysis conclusion can provide a model basis for the idle state of adjacent underground salt rock storage. For other projects with similar geological conditions, the proposed method can be used for modeling analysis and optimization in engineering practices.

Conflicts of interest/Competing interests

We declare that we do not have any commercial or associative interest that represents a conflict of interest in connection with the work submitted.

Availability of data and material

The datasets used or analysed during the current study are available from the corresponding author on reasonable request.

References

Bakhtiari, M., Shad, S., Zivar, D., & Razaghi, N. 2021. Coupled hydro-mechanical analysis of underground gas storage at Sarajeh field, Qom formation, Iran. *Journal of Natural Gas Science and Engineering*, 92: 103996. <https://doi.org/10.1016/j.jngse.2021.103996>

Chen, S.M., Wu, A.X., Wang, Y.M., Chen, X. 2017. Optimization research on slope structure parameters in broken rock conditions based on the response surface method. *Chinese Journal of Rock Mechanics and Engineering*, 36(S1): 3499-3508. Doi: 10.13722/j.cnki.jrme.2016.0715.

Dai, Y.H., Chen, W.Z., Yang, C.H., Tan, X.J., Jiang, X.L. 2009. A study of model test of Jintan rock salt gas storage's operation. *Rock and Soil Mechanics*, 30(12): 3574-3580. Doi: 10.16285/j.rsm.2009.12.029.

Jia, C., Zhang, K., Zhang, Q.Y., Xu, K. 2014. Research on multi-factor optimization of underground laminated salt rock storage group based on orthogonal experimental design. *Rock and Soil Mechanics*, 35(6): 1718-1726. Doi: 10.16285/j.rsm.2014.06.015.

Jiangsu provincial department of natural resources, 2021. Jintan, Changzhou "Using salt caves as storage". <http://zrzy.jiangsu.gov.cn/xwzx/ztcj/d52gsjdqr/jyiylyzy/2021/04/16101925960788.html>.

Jing, W.J., Yang, C.H., Li, L.M., Yuan, Z.Y., Shi, X.L., Li, Y.P. 2012. Sensitivity analysis of influence factors of cavity shrinkage risk in salt cavern gas storage. *Chinese Journal of Rock Mechanics and Engineering*, 31(9): 1804-1812.

Liu, J., Song, J., Zhang, Q.Y., Zhang, W.Q., Jia, C., Li, S.C., Yang, C.H. 2011. Numerical calculation and analysis of distance among salt rock underground gas storage caverns. *Chinese Journal of Rock Mechanics and Engineering*, 30(S2): 3413-3420.

Liu, W., Jiang, D., Chen, J., Daemen, J. J. K., Tang, K., & Wu, F. 2018. Comprehensive feasibility study of two-well-horizontal caverns for natural gas storage in thinly-bedded salt rocks in China. *Energy*, 143: 1006-1019. <https://doi.org/10.1016/j.energy.2017.10.126>

Liu, W., Muhammad, N., Chen, J., Spiers, C. J., Peach, C. J., Deyi, J., & Li, Y. 2016. Investigation on the permeability characteristics of bedded salt rocks and the tightness of natural gas caverns in such formations. *Journal of Natural Gas Science and Engineering*, 35(Part. A):468-482. <https://doi.org/10.1016/j.jngse.2016.07.072>

Liu, W., Zhang, Z., Chen, J., Jiang, D., Wu, F., Fan, J., & Li, Y. 2020. Feasibility evaluation of large-scale underground hydrogen storage in bedded salt rocks of China: A case study in Jiangsu province. *Energy*, 198: 117348. <https://doi.org/10.1016/j.energy.2020.117348>

Lu, J.L., Zhao, S.P., Sun, Y.P., Tang, H.J. 2018. Natural gas production peaks in China: Research and strategic proposals. *Natural Gas Industry*, 38(1): 1-9.

Moghadam, S. N., Nazokkar, K., Chalaturnyk, R. J., & Mirzabozorg, H. 2015. Parametric assessment of salt cavern performance using a creep model describing dilatancy and failure. *International Journal of Rock Mechanics and Mining Sciences*, 79: 250-267. <https://doi.org/10.1016/j.ijrmm.2015.06.012>

National Energy Administration, 2022. China's gas storage construction achieves original technical breakthrough. http://www.nea.gov.cn/2022-03/21/c_1310523065.htm.

Patroni, J. M. 2007. Life time of a natural gas storage well assessment of well-field maintenance cost. *Oil and Gas Science and Technology*, 62(3): 297-309. <https://doi.org/10.2516/ogst:2007025>

Shad, S., Razaghi, N., Zivar, D., & Mellat, S. 2022. Mechanical behavior of salt rocks: Geomechanical model. *Petroleum*. <https://doi.org/10.1016/j.petlm.2022.09.002>

Wang, T. T., Yan, X. Z., Yang, H. L., & Yang, X. J. 2011. Stability analysis of pillars between bedded salt cavern gas storages. *Journal of China Coal Society*, 36(5): 790-795.

Wanyan, Q., Xiao, Y., & Tang, N. 2019. Numerical simulation and experimental study on dissolving characteristics of layered salt rocks. *Chinese Journal of Chemical Engineering*, 27(5): 1030-1036. <https://doi.org/10.1016/j.cjche.2019.01.004>

Yang H.J. 2017. Construction key technologies and challenges of salt-cavern gas storage in China. *Oil & Gas Storage and Transportation*, 36(7): 747-753.

Zhang, H.B., Gao, K., Gou, Y.X., Ran, L.N., Li, K. 2022. Study on influence of interlayer on stability of injection-production operation of salt rock gas storage. *Journal of Safety Science and Technology*, 18(1): 29-35.

Zhang, Q.Y., Duan, K., Xiang, W., Yang, C.H., Cai, B., Xu, X.B., Jia, C., Liu, J. 2012. Three-dimensional rheological model test study of operational stability of deep laminated salt rock gas storage group under influence of extreme risk factors. *Chinese Journal of Rock Mechanics and Engineering*, 31(9): 1766-1775.

Zhang, Q.Y., Liu, D.J., Jia, C., Shen, X., Liu, J., Duan, K. 2009. Development of geomechanical model similitude material. *Rock and Soil Mechanics*, 30(12): 3581-3586. Doi: 10.16285/j.rsm.2009.12.002.

Zhou, B.K., Chen, X.Q., Tian, Y.C., Ma, D., Gong, G.H., Zhai, X.D., Deng, H.Z. 2021. Optimization of Slope Structure Parameters by Caving Method Based on Response Surface Method. *Metal Mine*, (3): 67-73. Doi: 10.19614/j.cnki.jsks.202103010.

Zivar, D., Kumar, S., & Foroozesh, J. 2021. Underground hydrogen storage: A comprehensive review. *International Journal of Hydrogen Energy*, 46(45): 23436-23462. <https://doi.org/10.1016/j.ijhydene.2020.08.138>



Original Research

Study on Floor Instability Law of Cemented Filling Mining above a Confined Aquifer

Jiaqi Wang^{a,b*},

^a School of Mines, China University of Mining and Technology, Xuzhou 221116, China

^a State Key Laboratory of Coal Resources and Safe Mining, China University of Mining and Technology, Xuzhou, Jiangsu, 221116, China

Received: 22 February 2022 • Accepted: 25 July 2023

A B S T R A C T

To solve the problem of floor water inrush in the process of coal mining on a confined aquifer and study the law of floor instability, a cemented filling mining method is proposed in the paper. Using river sand and cement as filling materials, the cementitious material with a concentration of 75% and cement content of 15% has the best flow and mechanical properties. Based on the elastic half-space theory and the bearing characteristics of the backfill, the mechanical model of floor stability is established, the critical criterion of floor instability is proposed, and the relationship between the failure depth of the floor and the location and pressure of the confined aquifer is obtained. The numerical simulation test scheme is designed, and the FLAC3D fluid-structure coupling element is used to explore the instability characteristics of the floor in the mining process. The research results show that the failure depth of the floor will gradually decrease with the increase of the strength of filling materials, the increase of aquifer distance, and the decrease of water pressure. The research results provide a useful reference for the study of the safe mining of coal resources in a confined aquifer.

Keywords: Confined aquifer, Cementitious materials, Filling mining, Floor, Numerical simulation test.

Introduction

According to the State Statistics Bureau, China's total energy consumption in 2021 was 4.49×10^9 t of standard coal, of which coal consumption accounts for 60.4% of the total energy consumption (Shen and Wang, 2023). Under such a large mining intensity, most mines have entered the deep level. Especially in the northern mines, they are seriously affected by the extremely thick Ordovician limestone aquifer at the bottom and are very prone to water inrush disasters. According to statistics, from 2015 to 2020, 133 water inrush disasters occurred on the coal seam floor of the northern mine (Yu et al., 2021). At present, China mainly uses drainage and depressurization method, curtain grouting methods, short-face mining methods, strip mining methods, double-face mining methods, segmented retreating mining methods, and filling mining methods to solve the water inrush of coal seam on confined water layer (Han et al. 2021; Sillitoe and Brogi, 2021; Yin et al., 2021). Among them, the drainage and depressurization method can't reduce the Ordovician limestone water with strong water abundance and sufficient supply; The production capacity of short face mining method is low, and the recovery rate of strip mining is low; The layout of the production system of the dou-

ble face mining is complex; The preparation time of segmented retreating mining method is long; Filling mining method can not only reduce the failure height of overburden but also reduce the failure depth of underlying strata. It is the safest and most reliable measure for mining on a confined aquifer.

Many scholars have done a lot of research on the methods of filling mining to prevent water inrush disasters. For example, Peng (Peng et al., 2021) used the high water material filling method to replace the strip coal pillar on the confined aquifer, analyzed the influence of filling body stability and floor failure, and finally verified the theoretical feasibility of this technology; Du (Du et al., 2021) analyzed the failure law and evolution characteristics of paste filled floor; and predicted the failure range and water inrush of the floor after mining Jia (Jia et al., 2021) quantitatively analyzed the control effect of strip filling replacement mining on surrounding rock deformation of working face and water diversion of the aquifer and Zhang (Zhang et al., 2021) used the methods of similarity simulation, theoretical research, and field practice to study the relationship between support and surrounding rock, ground pressure law of filling face and floor failure law under the condition of gangue filling mining.

* Corresponding author: 13852037975@163.com • <https://orcid.org/0000-0001-5679-0740>

The above research results have promoted the development of mining methods and theories on a confined aquifer, but its application effect is not obvious due to many factors such as filling material production cost, mining efficiency, and ecological protection. Therefore, taking the mining on the confined aquifer of the Zhaoguan energy mine as the background, this paper puts forward the cemented filling mining method to solve the above problems. The cementitious material composed of river sand and cement is designed, the optimal ratio of materials is studied, and the principle of water inrush from the mining floor on a confined aquifer is explained based on theoretical calculation. The numerical simulation test scheme is designed to explore the characteristics of floor instability in the mining process, and the influence law of cementitious material and aquifer distance on floor stability is obtained. The research results provide a useful reference for the study of the safe mining of coal resources on a confined aquifer and further enrich the rock stratum control theory of filling mining.

1. Test conditions

1.1. Geological conditions

Zhaoguan energy mine belongs to Qihe County, De Zhou City, Shandong Province. The minefield is located on the west edge of Dongtai Anticline of Taishan mountain in north China. The overall structural form is a monoclinic structure trending northeast and tending northwest, and the dip angle is generally 5~8°. Zhaoguan energy mine has a total area of 59.2 km², a design production capacity of 0.9 mt/a and a service life of 42.8 a. There are 8 minable coal seams in the mine. At present, 11 coal seams are designed to be mined. This coal seam is located above the elevation of -400 m, and the coal thickness is 0.25~2.92 m, with an average of 2 m. The density is 1.5 (g/cm³) and the minability coefficient is 0.8, which is a stable coal seam. The roof of coal seam 11 is quartzite, with an average thickness of 4 m, compressive strength of 104.2 MPa, and high rock integrity. It belongs to class IV's extremely stable floor. The floor is mudstone with compressive strength of 19.2 MPa, belonging to class I unstable bottom plate. In addition, there is Ordovician limestone 40 m below coal seam 11, which is dense and hard, with karst fractures developed, and the water pressure is about 4.5 MPa. Zhaoguan energy mine adopts cemented filling coal mining method to recover coal. The layout of the first mining face, production system, and rock stratum histogram is shown in Figure 1.

1.2. Mining conditions

The cemented filling coal mining technology designed in this project is based on the production of traditional longwall coal mining methods and uses the fully mechanized excavator to excavate the connecting roadway between the upper and lower roadway of the working face for coal mining. When one connecting roadway passes through the two roadways, the cemented filling material is used for filling, and the other connecting roadway is excavated at the same time. To increase production, multiple excavation faces are often arranged in the working face for mining. Compared with the traditional cemented filling face layout, this technology can realize the simultaneous operation of mining and filling, and reduce the length of the filling pipeline in goaf. It has the advantages of a simple system and high efficiency.

The specific mining process is divided into three stages: excavation of connecting roadway, coal transportation by belt conveyor, and connecting roadway filling. When a connecting roadway is excavated by the fully mechanized excavator, it will immediately be filled with cemented filling materials. Each connecting roadway shall be filled three times to ensure complete filling in the connecting roadway and reduce the lateral pressure on the filling retaining wall at the side of the lower roadway. To ensure that adjacent roadways will not be affected by mining, the two excavation faces shall be separated by more than three connecting roadways (Fahimifar and Zareifard, 2009; Liu et al., 2021; Guo et al., 2021), which is conducive to improving the stability of roof and floor during an unfilled period and reducing the risk of water inrush disaster. The cemented filling mining process is shown in Figure 2.

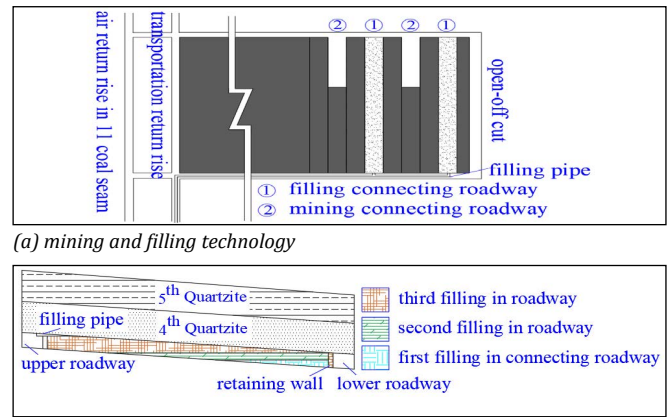


Figure 2. Cemented filling coal mining process

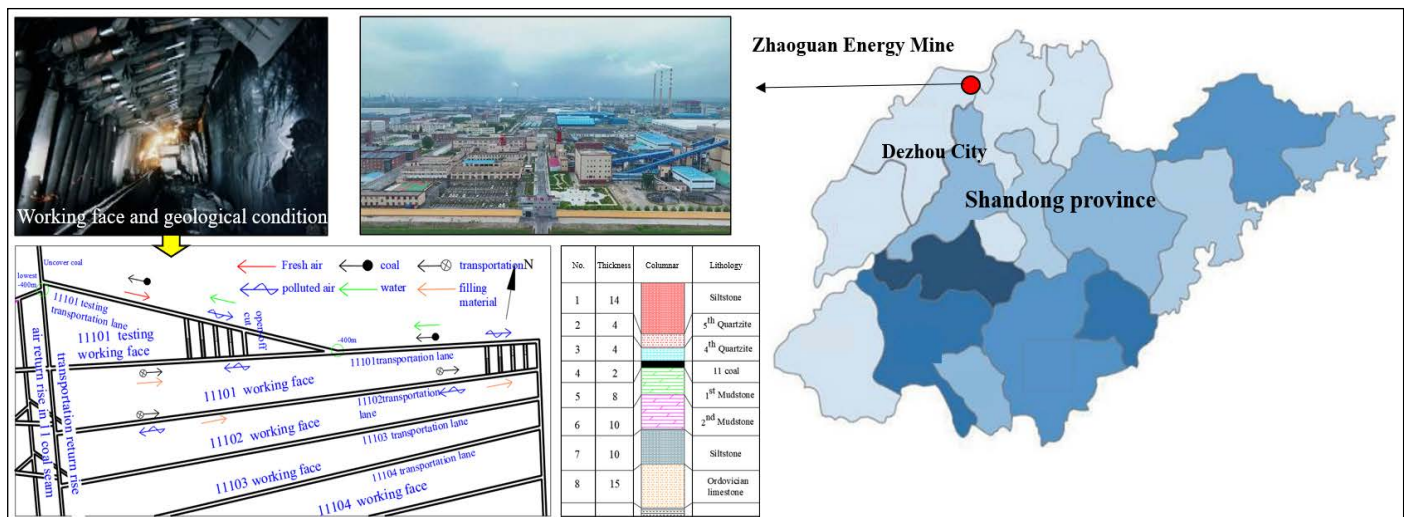


Figure 1. Working face layout, production system, and rock stratum histogram

2. Test material

The test material is river sand as aggregate and cement as a binder, which has the characteristics of convenient material acquisition and transportation. The main characteristics of cementitious materials are flow characteristics and mechanical properties. Among them, the mechanical properties are closely related to the stability of the working face floor, which needs to be studied. Six groups of proportioning were designed to study the flow characteristics and mechanical properties. The test scheme is shown in Table 1.

Table 1. Test scheme

Matching number	River sand/%	Cement/%	Concentration /%
S1	90	10	76
S2	90	10	75
S3	90	10	74
S4	90	10	73
S5	85	15	74
S6	95	5	74

2.1. Flow characteristic

The slump is used to describe the flow characteristics of cementitious materials, and the slump of cementitious materials with different ratios is obtained, as shown in Table 2. It can be seen from Table 2 that as the slurry concentration gradually decreases from 76%, the slump of the filling material first increases to the maximum value of 147mm, and then gradually falls. The slump value is the maximum when the slurry concentration is 75%. With the increase of the cement content, the slump of the filling material increases first and then tends to be stable, because the peaceability of the filling material is increased after the cement hydration reaction, increasing the slump. When the cement content reaches 10%, the influence of its content on the slump gradually decreases and the slump tends to be stable.

Table 2. Slump test results

Matching number	River sand/%	Cement/%	Concentration/%	Slump/mm
S1	90	10	76	131
S2	90	10	75	147
S3	90	10	74	128
S4	90	10	72	117
S5	85	15	75	138
S6	95	5	75	96

2.2. Mechanical properties

The cemented filling material is pumped to the goaf to maintain the good stability of the surrounding rock. A reasonable ratio can prevent the destruction of the floor, produce water inrush and support the roof. The filling materials of six schemes are made into standard samples, cured for 28 d, and tested for the stress-strain curves. The samples and test curves are shown in Figure 3 and Figure 4. It can be seen from Figure 4 that the strength of cementitious material from high to low is $S6 < S2 < S4 < S1 < S3 < S5$, which are 0.55 MPa, 1.22 MPa, 1.24 MPa, 1.42 MPa, 1.49 MPa, and 2.02 MPa respectively. Cementitious materials with a concentration of 75% and a cement content of 15% shall be chosen.



Figure 3. Filling material

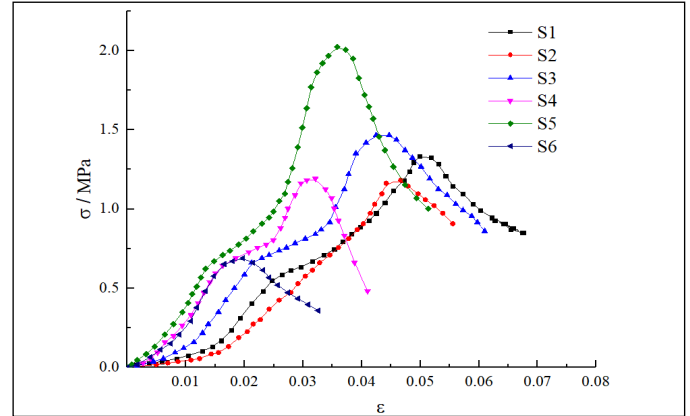


Figure 4. Stress-strain curve of filling material sample

3. Test principle

A mechanical model is established to study the water inrush principle of the floor on the confined aquifer. According to the literature (Batista Rodriguez et al., 2021; Wang et al. 2021; Xu et al., 2021), after mining, the floor rock near the end of the working face and the inner side of the goaf is greatly affected by the shear failure, and water inrush is very easy to occur in these places. Therefore, the filling mining model is established along the advancing direction of the longwall face, as shown in Figure 5. Analyze the stability of the floor (Fu and Wang., 2021; Wu et al., 2021; Ning et al., 2021), in the figure, L_2 is the influence range of coal wall support stress in front of the longwall working face, L_1 is the total width of the filling connecting roadway behind the solid coal, l_a is the width of the connecting roadway, and q_0 is the vertical load that the filling body can bear (taken as 2.18 MPa), γh is the overburden load, k is the stress concentration factor of the front coal wall, P is the pressure of the confined aquifer, and its distance from the coal seam floor is h_0 .

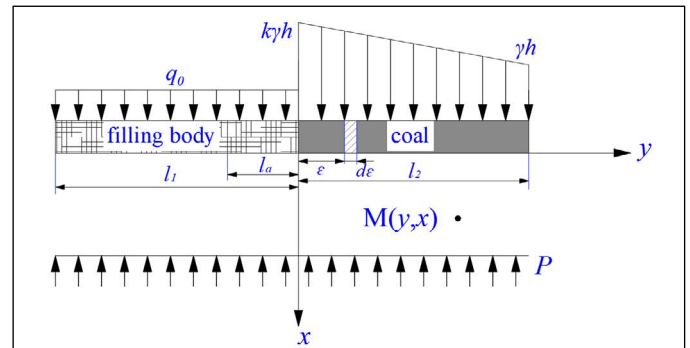


Figure 5. Depth failure model of floor

Then the model roof stress function is:

$$q(\varepsilon) = \begin{cases} q_0 & \varepsilon \in [0, l_1) \\ -\gamma h \left(\frac{1-k}{l_2} \varepsilon + k \right) & \varepsilon \in [l_1, l_2) \end{cases} \quad (1)$$

The rock strata below the coal seam floor are regarded as isotropic and homogeneous linear deformation bodies. According to the elastic half-space theory (Li et al., 2021; Nam and Bobet, 2006; Ma et al., 2021), the stress state in the floor rock stratum belongs to the plane strain problem, by taking the differential line segment $d\varepsilon$, the additional stress generated by the roof stress on any point $M(x, y)$ of the floor is calculated as follows:

$$\begin{cases} ds_x = \frac{2qd\varepsilon}{\rho} \frac{x^3}{[x^2 + (y-e)^2]^2} \\ ds_y = \frac{2qd\varepsilon}{\rho} \frac{x(y-e)^2}{[x^2 + (y-e)^2]^2} \\ dt_{xy} = \frac{2qd\varepsilon}{\rho} \frac{x^2(y-e)}{[x^2 + (y-e)^2]^2} \end{cases} \quad (2)$$

The stress component function at any point of the floor obtained by integration is:

$$\begin{cases} s_x = \frac{2}{\rho} \left(\int_{-l_1}^0 \frac{-q_0 x^3 d\varepsilon}{[x^2 + (y-e)^2]^2} + \int_0^{l_2} -gh \left[\frac{(1-k)}{l_2} e + k \right] \frac{x^3 d\varepsilon}{[x^2 + (y-e)^2]^2} - \int_{-l_1}^{l_2} \frac{P(h_0 - x)^3 d\varepsilon}{[(h_0 - x)^2 + (y-e)^2]^2} \right) \\ s_y = \frac{2}{\rho} \left(\int_{-l_1}^0 \frac{-q_0 x(y-e)^2 d\varepsilon}{[x^2 + (y-e)^2]^2} + \int_0^{l_2} -gh \left[\frac{(1-k)}{l_2} e + k \right] \frac{x(y-e)^2 d\varepsilon}{[x^2 + (y-e)^2]^2} - \int_{-l_1}^{l_2} \frac{P(h_0 - x)(y-e)^2 d\varepsilon}{[(h_0 - x)^2 + (y-e)^2]^2} \right) \\ t_{xy} = \frac{2}{\rho} \left(\int_{-l_1}^0 \frac{-q_0 x^2(y-e) d\varepsilon}{[x^2 + (y-e)^2]^2} + \int_0^{l_2} -gh \left[\frac{(1-k)}{l_2} e + k \right] \frac{x^2(y-e) d\varepsilon}{[x^2 + (y-e)^2]^2} - \int_{-l_1}^{l_2} \frac{P(h_0 - x)^2(y-e) d\varepsilon}{[(h_0 - x)^2 + (y-e)^2]^2} \right) \end{cases} \quad (3)$$

Using Coulomb Moore criterion, the maximum shear stress at any point under the floor can be obtained as follows:

$$t_{\max} = \sqrt{t_{xy}^2 + \frac{(s_x - s_y)^2}{2}} \quad (4)$$

It can be seen that when the stress at any point of the floor reaches or exceeds its strength, the point will yield failure. The failure criterion of any point below the floor is established as follows:

$$\left(\frac{s_x + s_y}{2} \tan j + c \right) / \sqrt{\tan^2 j + 1} \geq t_{\max} \quad (5)$$

Then the instability judgment function of filling coal mining floor is:

$$F(x, y) = \left(\frac{s_x - s_y}{2} \tan j + c \right) / \sqrt{\tan^2 j + 1} - t_{\max} \quad (6)$$

When $f(x, y) < 0$, the lower point of the floor is in a yield failure state. Bring the mechanical parameters of Zhaoguan energy mine rock into Equation (6), and take the friction angle in the floor $\varphi = 30^\circ$, cohesion $c = 2.8$ MPa, the range of influence of support pressure on the front coal body $l_2 = 40$ m, and stress concentration factor $k = 2.1$. The critical state curve of floor instability can be made, as shown in Figure 6.

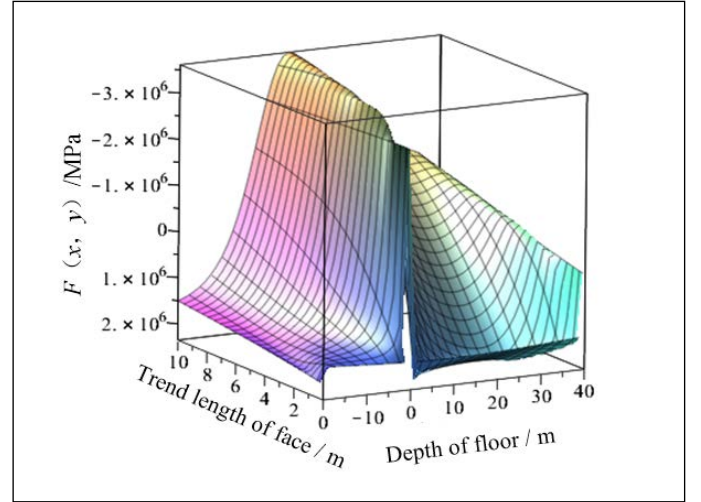


Figure 6. Distribution of function $f(x, y)$

It can be seen from Figure 6 that the maximum failure depth of the coal seam floor is 12.4 m, which occurs 3.49 m behind the solid coal. The maximum depth failure point of the bottom plate is still 37 m away from the confined aquifer. At the same time, the analysis of Equation (6) shows that the strength of the filling body, the location of the confined aquifer, and the water pressure of the aquifer have a great impact on the stability of the floor.

4. Test method and scheme

4.1. Test method

FLAC3D fluid-structure coupling model is used to analyze the law of floor instability under the influence of mining and confined aquifer. In the FLAC3D fluid-structure coupling module, the rock mass is regarded as a porous medium, and the fluid meets Darcy's law and Biot's classical seepage equation (Duan and Zhao, 2021; Zhang et al., 2021; Shi et al., 2021). After entering the fluid-structure coupling calculation mode, the reasonable selection of rock mass and fluid seepage parameters has a great impact on the calculation results. According to the borehole histogram of the Zhaoguan energy mining area and the physical mechanics and seepage parameters of different lithologies in the North China mining area, the numerical simulated coal and rock mass physical mechanics parameters and seepage parameters are designed in Table 3. The mohr-Coulomb constitutive model is adopted for rock mass and fluid is adopted for the fluid_ iso isotropic model.

Table 3. The parameters of physical and mechanical coal and rock mass and percolation

Lithology	Bulk density / Kg·m ⁻³	tensile strength / MPa	internal friction angle	cohesion / MPa	Elastic model / GPa	Poisson's ratio	Permeability coefficient / m ² ·Pa ⁻¹ ·sec ⁻¹	Fluid density / Kg·m ⁻³
Siltstone	2500	0.3	35	3.2	6	3.2	1e-10	1e3
4 th Quartzite	2600	0.5	37	3.5	5	2.0	1e-8	1e3
5 th Quartzite	2600	0.5	40	8.1	13.9	9.1	1e-8	1e3
11coal	2573	0.08	25	0.5	0.2	0.1	1e-7	1e3
1 st Mudstone	2500	0.4	35	2.2	2.25	0.5	1e-10	1e3
2 nd Mudstone	2520	0.4	35	2.2	2.25	0.5	1e-10	1e3
Siltstone	2500	0.3	37	3.2	6	3.2	1e-9	1e3
Ordovician limestone	2610	0.3	35	3.6	3.3	2.0	1e-8	1e3

The numerical calculation model of cemented filling mining is established, and the size of the model is 100x120x67 m. Fully constrained boundary conditions are adopted at the bottom and around the model, vertical stress of 7.5 MPa is applied at the top to simulate the pressure of overburden on the model and a permeable seepage boundary with a fixed water pressure of 4.5 MPa is applied at the bottom to simulate the pressure of confined aquifer. After excavation, the goaf adopts drainage boundary conditions (Ma et al., 2019; Ma et al., 2019; Ma et al., 2021), and the model is established as shown in Figure 7. ① ~ ④ in the Figure 7 is the first step of filling and mining to the fourth step of filling and mining. The width of each connecting roadway is 4.5 m.

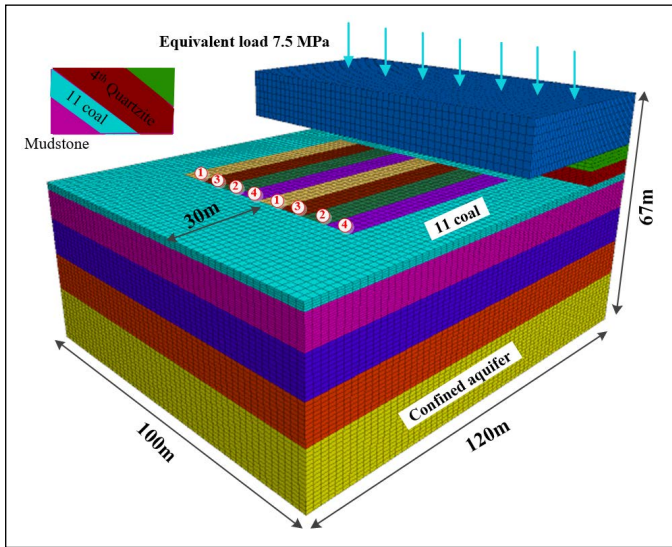


Figure 7. Numerical model of cemented filling mining

4.2. Test scheme

After the model is established, the initial balance calculation is carried out, and then mining and filling are carried out. The design working face adopts two excavation faces for mining, and the overall mining sequence is Mining ① - filling ① - mining ② - filling ② - mining ③ - filling ③ - mining ④. In the mining process of working face, the development of a plastic zone of floor and pore water pressure are observed and analyzed.

In the subsequent tests, three parameters of backfill strength, aquifer distance, and water pressure were adjusted to analyze their influence on the stability of the floor. The strength of the filling body is selected from six proportioning schemes such as S6, S2, S4, S1, S3, and S5. The aquifer distance is designed as 10 m, 20 m, 30 m, 40 m, 50 m, 60 m, 70 m, 80 m, and 90 m. The water pressure of the aquifer is 0 MPa, 0.5 MPa, 1.0 MPa, 1.5 MPa, 2.0 MPa, 2.5 MPa, 3.0 MPa, 3.5 Mpa, 4.0 Mpa, 4.5 MPa and 5 MPa respectively.

5. Test results and discussion

5.1. Law of floor instability during cemented filling mining

During the mining cycle, the state zone module is used to analyze the plastic zone of the excavation and filling area, and the distribution characteristics of the plastic failure zone of the floor are obtained as shown in Figure 8.

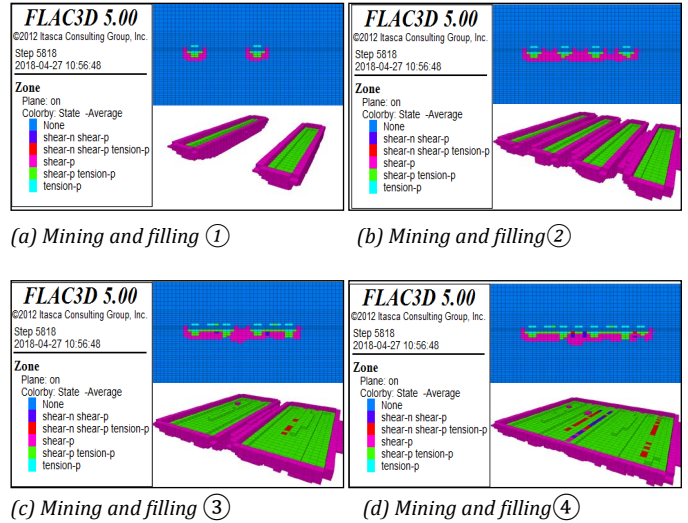


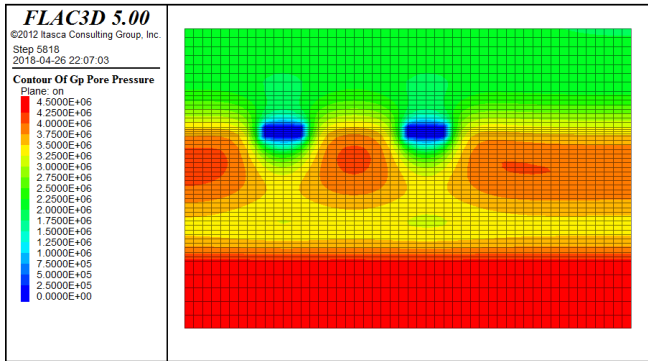
Figure 8. Distribution characteristics of plastic failure of the floor

It can be seen from Figure 8 that the failure type of rock mass in the process of excavation and filling is mainly shear failure. With the continuous excavation and filling of connecting roadways, the plastic failure area of the floor rock mass in the mining area is continuously connected and deepened. When excavating and filling ①, the maximum failure depth of the plastic area of the coal seam floor is 4 m and symmetrically distributed. When excavating and filling ④, The maximum damage depth of the coal seam floor is 7 m, which occurs in the middle of the mining area and is far away from the Ordovician limestone. The water diversion failure zone cannot relate to the uplift zone of the confined water layer (Yan et al., 2021; Zhang and Wang, 2007; Zhang et al., 2015), which eliminates the risk of water inrush.

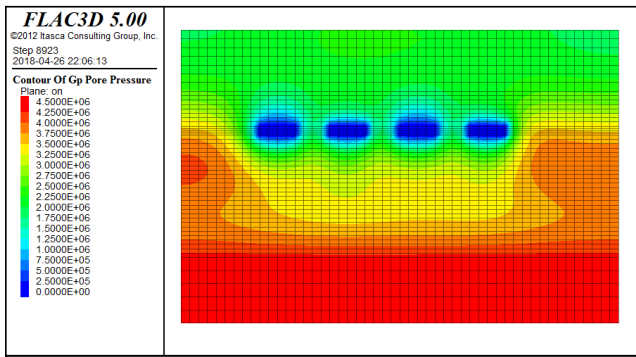
At the same time, when a connecting roadway is excavated, the coal near the roadway is vulnerable to shear damage. The “skip mining” method is adopted to mine at a far position from the mined connecting roadway. After the filling body is stable, mining at a closer position can effectively prevent the occurrence of coal wall caving and other phenomena. As the roof lithology of the Zhaoguan energy mine is limestone with good stability, and the above methods are used for coal mining, the roof stability is good. Tension failure occurs only in the middle of the connecting roadway, and the depth is less than 1 m.

4.2.2. Analysis of pore water pressure in mining

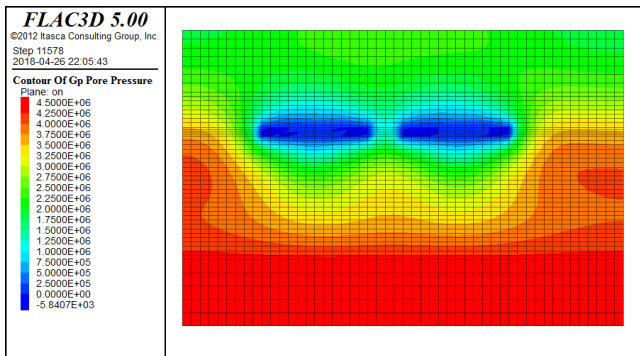
In the process of mining, the pore water pressure of the model is analyzed by calling the pore pressure module, and the pore water pressure distribution is shown in Figure 9.



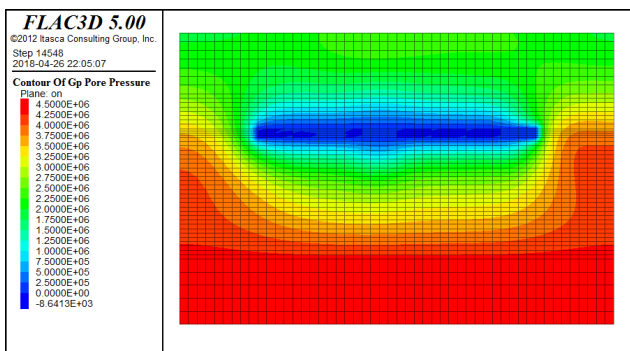
(a) Mining and filling ①



(b) Mining and filling ②



(c) Mining and filling ③



(d) Mining and filling ④

Figure 9. Pore water pressure distribution

It can be seen from Figure 9 that the pore water pressure increases fastest on both sides of the connecting roadway and the mining area. It can be seen that water inrush disasters are very easy to occur near the goaf and the mining area boundary, and attention should be paid to the prevention and control of water inrush in this area. In addition, the water-conducting boundary of bedrock (Zhou et al., 2016; Zhang et al., 2015; Yin et al., 2020) always exceeds the mining boundary, and the seepage velocity of the lower rock stratum is always greater than that of the upper rock stratum.

5.2. Law of floor instability under the influence of strength of cementitious material

The influence law of cementitious material on the failure depth of the floor is obtained, as shown in Figure 10. As can be seen from Figure 10, as the strength of the filling body gradually increases, the failure depth of the floor gradually decreases. When the strength of the filling body is 0.55 MPa, 1.22 MPa, 1.24 MPa, 1.42 MPa, 1.49 MPa, and 2.02 MPa, the failure depth of the floor is 14.02 m, 12.89 m, 10.34 m, 9.22 m, 8.89 m, and 8.02 m respectively. Therefore, filling cementitious materials can effectively prevent water inrush.

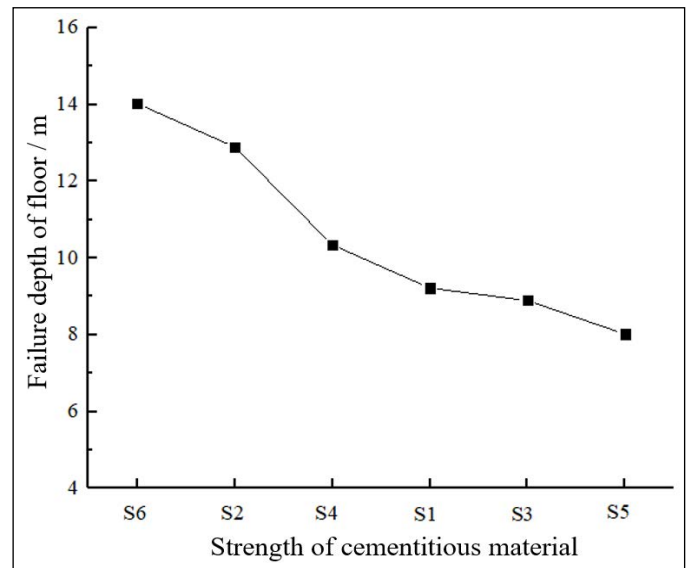


Figure 10. Effect of the strength of cementitious material on failure depth of the floor

5.3. Law of floor instability under the influence of aquifer distance and water pressure

The influence law of aquifer distance on floor failure depth is obtained, as shown in Figure 11. The influence law of water pressure on the failure depth of the floor is also obtained, as shown in Figure 12. As can be seen from Figures 11 and 12, with the continuous increase of the pressure of the confined aquifer, the failure depth of the bottom plate gradually increases. When the pressure of the confined aquifer is greater than 2 MPa, the failure depth of the bottom plate increases obviously. With the gradual increase of the distance between the confined aquifer and the coal seam, the damage depth of the floor gradually decreases. However, it can be seen that the floor of the working face is always greatly affected by the confined aquifer when the aquifer depth increases from 10 m to 90 m. It can be seen that the problem of the confined aquifer cannot be ignored in the safe mining of coal mines, and the guarantee measures for the safe mining on the confined aquifer should always be taken.

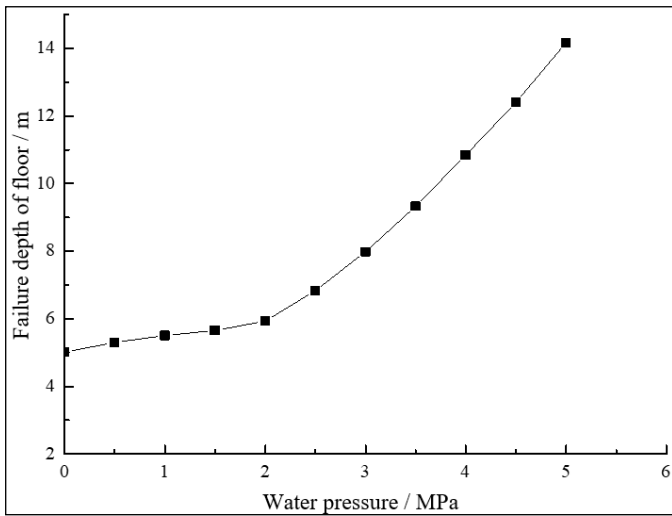


Figure 11. Effect of water pressure on failure depth of the floor

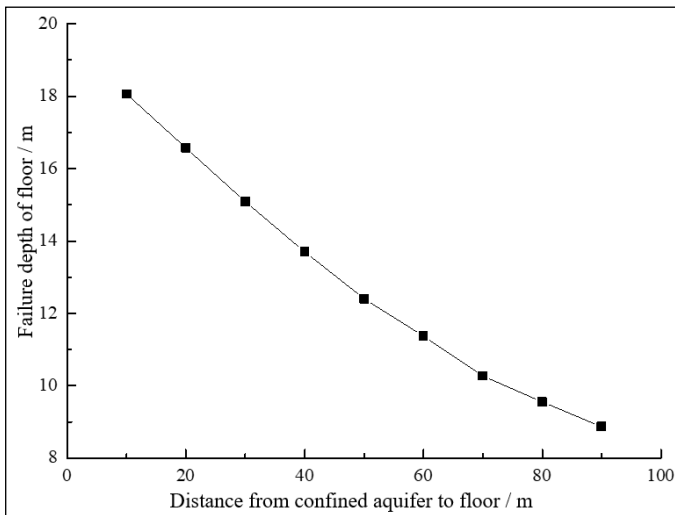


Fig. 12 Effect of confined aquifer depth on failure depth of the floor

6. Conclusion

To realize safe mining above the confined aquifer, this paper puts forward the cemented filling mining method, designs the best ratio of cemented materials, and explains the principle of water inrush from the mining floor on the confined aquifer based on theoretical calculation. The numerical simulation test scheme is designed to explore the characteristics of floor instability in the mining process. The specific conclusions are as follows:

(1) Given the technical problems of mining on the confined aquifer in the Zhaoguan energy mine, a cemented filling mining method is proposed. Combined with the actual conditions of the mining area, the filling material ratio of Yellow River Sediment: Cement = 0.85:0.15 is designed, the slump reaches 138 mm and the strength reaches 2.02 MPa.

(2) Based on the elastic space half-space theory, the mechanical model of floor instability in cemented filling coal mining is established, the critical criterion formula of floor instability is deduced, the principle of floor instability on confined aquifer is explained, and the maximum failure depth of working face floor is determined to be 12.4 m. At the same time, it is obtained that the strength of cemented material, aquifer distance, and aquifer water pressure are the main factors affecting floor stability.

(3) Based on the analysis of the calculation results of the fluid-structure coupling numerical model, it can be seen that the surrounding rock damage during the excavation and filling of the connecting roadway is mainly shear damage, and water inrush is very easy to occur in the goaf and the boundary of the mining area. At the same time, with the increase in the strength of cementitious material, the increase in aquifer distance, and the decrease in water pressure, the failure depth of the floor decreases gradually.

(4) The numerical simulation test shows that when the aquifer distance is 40 m, the water pressure is 4.5 MPa and the strength of cementitious material is 2.02 MPa, the failure depth of the floor is far less than 15 m, which is consistent with the theoretical settlement results, which proves that this method can effectively solve the problem of floor water inrush.

Data availability statement

The original contributions presented in the study are included in the article, further inquiries can be directed to the corresponding author.

Author contributions

Jiaqi Wang: Conceptualization, Model investigation, Data curation, Writing - original draft.

Acknowledgments

Thanks to the staff of Zhaoguan energy mine.

Conflicts of interest

The author declare no conflicts of interest.

References

- Batista-Rodriguez, J. A., Perez-Flores, M. A., Almaguer-Carmenates, Y., Blanco-Moreno, J. A., Lopez-Saucedo, F. D. J., & Batista-Cruz, R. Y. 2021. Using electrical resistivity tomography to evaluate the relationship between groundwater potential and tectonism in northeast Mexico. *Revista Mexicana de Ciencias Geologicas*, 38(1), 18-28.
- Du, Y., Liu, W., Meng, X., Pang, L., & Han, M. 2021. Effect of Crack Propagation on Mining-Induced Delayer Water Inrush Hazard of Hidden Fault. *Geofluids*, 2021.
- Duan, H., & Zhao, L. 2021. New evaluation and prediction method to determine the risk of water inrush from mining coal seam floor. *Environmental Earth Sciences*, 80(1), 1-13.
- Fu, B., & Wang, B. 2021. An Influence Study of Face Length Effect on Floor Stability under Water-Rock Coupling Action. *Geofluids*, 2021.
- Fahimifar, A., & Zareifard, M. R. 2009. A theoretical solution for analysis of tunnels below groundwater considering the hydraulic-mechanical coupling. *Tunnelling and Underground Space Technology*, 24(6), 634-646.
- Guo, J., Zhang, Q., Li, Q., & Chen, Z. 2021. Study on permeability evolution mechanism of aquifer coal seam roof sandstone under plastic flow. *Geomechanics and Geophysics for Geo-Energy and Geo-Resources*, 7(3), 1-22.
- Han, D., Currell, M. J., & Guo, H. 2021. Controls on distributions of sulphate, fluoride, and salinity in aquitard porewater from the North China Plain: Long-term implications for groundwater quality. *Journal of Hydrology*, 603, 126828.
- Jia, J., Hao, X., Zhao, G., Li, Y., Chuai, X., Huang, L., & Zhan, R. 2021. Evolution analysis of microseismic events before and after mining through large-scale weak zone with high confined water. *Advances in Civil Engineering*, 2021.

- Li, A., Mu, Q., Ma, L., Liu, C., Wang, S., Wang, F., & Mou, L. 2021. Numerical Analysis of the Water-blocking Performance of a Floor with a Composite Structure under Fluid–solid Coupling. *Mine Water and the Environment*, 40(2), 479-496.
- Liu, Z., Dong, S., Wang, H., Wang, X., Nan, S., & Liu, D. 2021. Macroscopic and mesoscopic development characteristics of the top strata of Middle Ordovician limestone in the Hanxing mining area. *Environmental Earth Sciences*, 80(16), 1-17.
- Ma, K., Sun, X. Y., Tang, C. A., Yuan, F. Z., Wang, S. J., & Chen, T. 2021. Floor water inrush analysis based on mechanical failure characters and microseismic monitoring. *Tunnelling and Underground Space Technology*, 108, 103698.
- Ma, D., H Duan, Liu, J., Li, X., & Zhou, Z. 2019. The role of gangue on the mitigation of mining-induced hazards and environmental pollution: an experimental investigation. *Science of the Total Environment*, 664(MAY 10), 436-448. doi: 10.1016/j.scitotenv.2019.02.059
- Ma, D., Duan, H., Li, X., Li, Z., Zhou, Z., & Li, T. 2019. Effects of seepage-induced erosion on nonlinear hydraulic properties of broken red sandstones. *Tunnelling and Underground Space Technology*, 91(SEP.), 102993. doi: 10.1016/j.tust.2019.102993
- Ma, D., Zhang, J., Duan, H., Huang, Y., & Zhou, N. 2021. Reutilization of gangue wastes in underground backfilling mining: overburden aquifer protection. *Chemosphere*, 264(Pt 1), 128400. doi: 10.1016/j.chemosphere.2020.128400
- Ning, S., Zhu, W., Yi, X., & Wang, L. 2021. Evolution Law of Floor Fracture Zone above a Confined Aquifer Using Backfill Replacement Mining Technology. *Geofluids*, 2021.
- Nam, S. W., & Bobet, A. 2006. Liner stresses in deep tunnels below the water table. *Tunnelling and Underground Space Technology incorporating Trenchless Technology Research*, 21(6), 626-635.
- Peng, Z., Chen, L., Hou, X., Ou, Q., Zhang, J., & Chen, Y. 2021. Risk assessment of water inrush under an unconsolidated, confined aquifer: the application of GIS and information value model in the Qidong Coal Mine, China. *Earth Science Informatics*, 1-14.
- Shen, S. M., & Wang, H. Y. 2023. Asymmetric Multifractal Analysis of the Chinese Energy Futures and Energy Stock Markets under the Impact of COVID-19. *Fluctuation and Noise Letters*, 22(01), 2350002.
- Sillitoe, R. H., & Brogi, A. 2021. Geothermal systems in the northern apennines, italy: modern analogues of carlin-style gold deposits. *Economic Geology*, 116(7), 1491-1501.
- Shi, X., Zhou, H., Sun, X., Cao, Z., & Zhao, Q. 2021. Floor damage mechanism with cemented paste backfill mining method. *Arabian Journal of Geosciences*, 14(2), 1-9.
- Wang, Z., Li, W., & Hu, Y. 2021. Experimental study on mechanical behavior, permeability, and damage characteristics of Jurassic sandstone under varying stress paths. *Bulletin of Engineering Geology and the Environment*, 1-17.
- Wu, J., Jing, H., Meng, Q., Yin, Q., & Yu, L. 2021. Assessment of cemented waste rock backfill for recycling gangue and controlling strata: creep experiments and models. *Environmental Science and Pollution Research*, 1-17.
- Xu, C., Lu, C., & Wang, J. 2021. Interval uncertainty analysis of a confined aquifer. *Scientific reports*, 11(1), 1-5.
- Yu, G. F., Yuan, L., & Ren, B. 2021. Big data cloud platform for monitoring and early warning of water disaster from coal floor and its application feasibility in Huaihe Energy Group [J/OL]. *Journal of China Coal Society*, 08-05.
- Yin, H., Xu, B., Yin, S., Tian, W., Yao, H., & Meng, H. 2021. Prevention of Water Inrushes in Deep Coal Mining over the Ordovician Aquifer: A Case Study in the Wutongzhuang Coal Mine of China. *Geofluids*, 2021.
- Yan, H., Zhang, J., Li, B., & Zhu, C. 2021. Crack propagation patterns and factors controlling complex crack network formation in coal bodies during tri-axial supercritical carbon dioxide fracturing. *Fuel*, 286, 119381. doi: 10.1016/j.fuel.2020.119381
- Yin, H., Zhao, C., Zhai, Y., Sang, S., Zhao, H., Li, S., ... & Zhuang, X. 2020. Application of comprehensive support techniques to roadway tunneling in vicinity of Ordovician carbonate confined aquifers under complicated tectonic conditions. *Carbonates and Evaporites*, 35(4), 1-14.
- Zhang, J., Guo, L., Mu, W., Liu, S., & Zhao, D. 2021. Water-inrush Risk through Fault Zones with Multiple Karst Aquifers Underlying the Coal Floor: A Case Study in the Liuzhuang Coal Mine, Southern China. *Mine Water and the Environment*, 1-11.
- Zhang, Y. 2021. Mechanism of Water Inrush of a Deep Mining Floor Based on Coupled Mining Pressure and Confined Pressure. *Mine Water and the Environment*, 40(2), 366-377.
- Zhang, Q. L., & Wang, X. M. 2007. Performance of cemented coal gangue backfill. *Journal of Central South University of Technology*, 14(2), 216-219. doi: 10.1007/s11771-007-0043-y
- Zhang, J., Qiang, Z., Sun, Q., Gao, R., Germain, D., & Abro, S. 2015. Surface subsidence control theory and application to backfill coal mining technology. *Environmental Earth Sciences*, 74(2), 1439-1448. doi: 10.1007/s12665-015-4133-0
- Zhou N, Han X, Zhang J, et al. 2016. Compressive deformation and energy dissipation of crushed coal gangue[J]. *Powder Technology*, 297:220–228. doi: 10.1016/j.powtec.2016.04.026



Original Research

Comparison of Conditioned Radial Basis Function Approach and Kriging: Estimation of Calorific Value in a Coal Field

Firat Atalay^{a,*}

^a Hacettepe University, Mining Engineering Department, Ankara, Türkiye

Received: 16 June 2023 • Accepted: 31 July 2023

A B S T R A C T

Due to low production cost, coal is still the most important source of electricity production worldwide. This important position of coal also makes the evaluation of coal resources important. One of the most important attributes to be assessed in this evaluation is estimating the calorific value distribution of deposit. In geostatistical estimation currently kriging and its variants are being used widely. Alternatively new techniques are being developed and one of them is the Radial Based Functions based method. In this study, Conditioned Radial Basis Function (CRBF) is used to estimate the calorific value distribution of a coal deposit while estimations are also performed with ordinary kriging (OK). Results of both estimation methods are compared with respect to composite calorific values. Results show that CRBF produced a higher estimation range than OK with closer mean to composite. However, like OK, results are still smoother than the composite values.

Keywords: Coal, Radial basis function, Kriging, Geostatistics

Introduction

Coal is the most important natural resource used for electricity generation in the world, with a share of 38.3% in electrical energy production. In Türkiye, 37.1% of the electrical energy is covered by coal, like the world, and it takes the status of the most important electrical energy source for Türkiye which is the 19th biggest economy in the world. The total coal reserve of the world is approximately 1.07 trillion tons with annual coal consumption of 8 billion tons. The relationship between reserves and consumption in the world is similar in Türkiye while total coal reserve of the Türkiye is 19.32 billion tons, while coal consumption is around 115 million tons (Turkish Coal Enterprises, 2021). As can be seen, when the reserve and consumption rates are examined both in the world and in Türkiye, coal is the most important natural resource that supports sustainable electricity generation today. For this reason, it is of great importance to reveal the coal resources.

The most important variable in coal resources is the calorific value (Chelgani, 2021). A coal asset with insufficient calorific value cannot be considered as a coal source. The calorific value in coal beds varies depending on the location (Olea et al., 2011). It is not possible to take steps such as feasibility and production plan-

ning without modeling this variability. For this reason, the calorific value variability in coal resources and the amount of coal resources have been the subject of many studies. Fang et al. (1980) examined the usability of geostatistical methods in the estimation of coal resources. In addition, Srivastava (2013) noted the widespread use of geostatistical methods in revealing the spatial variability of coal resources and referred to many related studies. Demirel et al. (2000) performed resource estimation of the coal field in the Çanakçı, which is located in Ermenek region, using the kriging method. Tercan and Karayiğit (2001), carried out coal resource estimation studies in Kalburçayırı in Sivas - Kangal region and Tercan et al. (2013) revealed some coal resources in Western Anatolia. Whateley et al. (1997) coal resource estimations with different methods and compared the methods in the Turgut coal deposit located in Muğla-Yatağan. Inaner et al. (2008) on the other hand, made the resource estimation of the Bayır field in Yatağan. Ertunc et al. (2013) estimated the variability of calorific value in coal beds which was modeled by covariance-matched kriging. On the other hand, Afzal (2018) made a coal resource estimation using kriging and inverse distance methods in Parvadeh coal deposit in Iran and evaluated the results. Jeuken et al. (2020) compared the inverse distance weighting and kriging techniques in a coal

* Corresponding author: atalay@hacettepe.edu.tr • <https://orcid.org/0000-0001-6349-7745>

deposit in Queensland, Australia. They made resource estimation using many methods. Sideri et al. (2020) estimated the mean lower calorific value of coal by using ordinary kriging methods. In this study, methods such as ordinary kriging, covariance-matching kriging and inverse distance weighting methods were used. The methods used in coal resource estimation are still in the development stage. For example, Atalay and Tercan (2017) conducted coal resource estimation with Copulas. In the framework of newly developing approaches, radial basis function estimation has never been used in the estimation of coal resources (Atalay et al. 2021).

In mineral resource estimation, in addition to classical methods such as inverse distance and kriging, relatively new advanced methods such as radial basis functions are also used. Due to the nature of the method, estimations made with radial basis functions do not meet the requirements for resource estimation to be positive definite and the estimation to be within a certain range. For this reason, direct estimation with radial basis functions will generate erroneous results. For this reason, a new approach is needed to make estimation with radial basis functions.

Since the radial basis function cannot be used in direct estimation safely, in this study, estimation is made using the conditioned radial basis function developed using radial basis functions and results were compared with kriging. For the purpose of estimation, first of all, a 3D model of the coal bed was created. After that, the kriging steps were applied. For kriging, the experimental variogram was calculated and the model variogram was fitted and the calorific value was estimated by ordinary kriging. After the kriging process, the calorific value of the coal was estimated by the conditioned radial basis function. As a result, kriging and the developed conditioned radial basis function interpolation are compared in terms of summary statistics.

1. Method

1.1. Ordinary Kriging

Kriging is basically an interpolation method based on the minimization of error variances using distance-based variability. To perform estimation using kriging, the variability depending on the distance must first be determined (Thomas, 2013). Variability due to distance is usually obtained by calculating experimental variogram values. The experimental variogram is calculated as shown in Eq. 1 (Cressie,1990, Journel and Huijbregts, 1978)

$$\gamma(h) = \frac{1}{2N(h)} \sum_{i=1}^n (x_i - x_{i+h})^2 \tag{1}$$

Here; $\gamma(h)$ is experimental variogram, $N(h)$ is number of pairs and $(x_i - x_{i+h})$ is difference of pairs.

In general, experimental variogram calculation step is followed by model fitting step. Until now, many variogram models were developed like Gaussian, spherical, exponential. Among them, the spherical model is the most widely used one and is shown in Eq. 2.

$$\gamma(h) = C_o + C * \left[\frac{3h}{2a} - \frac{1}{2} \left(\frac{h}{a} \right)^3 \right] \tag{2}$$

Here; C_o is nugget effect, C is sill value, h is distance and a is range.

By fitting the variogram model, it is possible to set up kriging equations. The kriging method, like many other estimation methods, works by assigning weights to the data adjacent to the desired location (Eq. 3) (Pardo-Iquiza et al. 2013).

$$z(x_o) = \sum_{i=1}^n \lambda_i * z(x_i) \tag{3}$$

Here; $z(x_o)$ is estimation point, λ_i is estimation weight and $z(x_i)$ shows estimation location. Estimation methods differ from each other by calculating the estimation weight in a different way (Eq. 4) (Rossi and Deutsch 2013, Rossi and Deutsch, 2014).

$$\begin{cases} \sum_{i=1}^n \lambda_i * z(x_i) + \mu = \gamma(x_o, x_i) \\ \sum_{i=1}^n \lambda_i = 1 \end{cases}, i = 1, \dots, n \tag{4}$$

Here, μ is Lagrange multiplier and $\gamma(x_i, x_o)$ variogram value of that corresponds to distance between estimation point and sample point. As seen in Equation 4, the sum of the weights used in the estimation equals 1. A matrix equation that satisfies the conditions above is given in Eq. 5 (Myers,1992, Olea et al., 2011, Olea, 2012).

$$\begin{pmatrix} \gamma(x_1, x_1) & \gamma(x_1, x_2) & \dots & \gamma(x_1, x_n) & 1 \\ \gamma(x_2, x_1) & \gamma(x_2, x_2) & \dots & \gamma(x_2, x_n) & 1 \\ \dots & \dots & \dots & \dots & \dots \\ \gamma(x_n, x_1) & \gamma(x_n, x_2) & \dots & \gamma(x_n, x_n) & 1 \\ 1 & 1 & 1 & 1 & 0 \end{pmatrix} \begin{pmatrix} \lambda_1 \\ \lambda_2 \\ \dots \\ \lambda_n \\ \mu \end{pmatrix} = \begin{pmatrix} \gamma(x_o, x_1) \\ \gamma(x_o, x_2) \\ \dots \\ \gamma(x_o, x_n) \\ 1 \end{pmatrix} \tag{5}$$

By solving the kriging matrix equation, the estimation weights are calculated, and thus estimations can be performed by placing the unknown weights in Eq. 3.

1.2. Radial Basis Function

Radial basis functions are first introduced to estimate topography and other irregular surfaces while scattered data is available (Hardy, 1971). It is used for many applications in engineering problems in engineering and scientific problems while interpolation is one of them. Radial basis functions are effective tool for data interpolation problems (Schaback and Wendland,2001).

The main characteristic of the radial basis function is value of the function is changes monotonically with distance respect to central point (Orr, 1996). A radial basis function (RBF) can be defined as a function that takes values based on the distance from origin or center point (Eq. 6).

$$\phi(x) = \phi(\|x_i\|) \text{ or } \phi(x) = \phi(\|x_i - c\|) \tag{6}$$

Here $\phi(x)$ is radial function, $\|x\|$ is distance operator and c is center.

RBF is always positively defined even though some inputs are negative. In RBF distance is generally measured in Euclidean form. Most widely used RBFs are given in Table 1.

Table 1. Some radial basis functions (Schagen, 1979).

RBFs	$\phi(x)$
Gaussian	$e^{-(cr)^2}$
Multiquadric	$\sqrt{r^2 + c^2}$
Inverse Multiquadric	$\frac{1}{\sqrt{r^2 + c^2}}$
Inverse Quadratic	$\frac{1}{r^2 + c^2}$

In table 1 c and r parameters determine the shape of the function which affects the function output value. As seen from the table many alternative kernel functions are available. However, Gaussian kernel is the most widely used one.

Estimation with radial basis function, like in kriging, depends on the estimation of the weights associated with sampling points.

Although the method is quite similar to kriging, the only difference is that a radial basis function ϕ (II-II) processor is used instead of the variogram value of the distance between the $z(x_i)$ measurement values of the equation established on the left side of the matrix equation. Also, on the right side of the equation, the f interpolant is used in a similar way.

$$\sum_{i=1}^n \lambda_i * \phi(\|x_i - x_0\|) = f \tag{7}$$

In this case, the matrix equation yielded for the purpose of estimation is given in the Eq. 8.

$$\begin{bmatrix} \phi(\|x_1 - x_1\|) & \phi(\|x_2 - x_1\|) & \dots & \phi(\|x_n - x_1\|) \\ \phi(\|x_1 - x_2\|) & \phi(\|x_2 - x_2\|) & \dots & \phi(\|x_n - x_2\|) \\ \vdots & \vdots & \dots & \vdots \\ \phi(\|x_1 - x_n\|) & \phi(\|x_2 - x_n\|) & \dots & \phi(\|x_n - x_n\|) \end{bmatrix} \begin{bmatrix} \lambda_1 \\ \lambda_2 \\ \vdots \\ \lambda_n \end{bmatrix} = \begin{bmatrix} f(x_1) \\ f(x_2) \\ \vdots \\ f(x_n) \end{bmatrix} \tag{8}$$

In Eq. 7 the distance of all values to be used in the estimation is the value of the kernel function used, and λ_i represents the value of the function at the relevant distance. Accordingly, with the solution of the matrix equation for all λ_i s, that is, the weights to be used in the estimation, the estimation process is performed as in the Eq. 3.

The estimation of radial basis functions is in the range due to the nature of the operators. However, it is not possible for mineral resources to have a negative value. In addition, mineral resources reach a limited value. For example, the average calorie of the known best quality coal occurrences is around 8000 kCal/kg. As can be seen, the radial basis function that generates estimation results in the range of can not be used directly in mineral resource estimation. For this reason, the method should be adapted to mineral resource estimation.

1.3. Conditioned Radial Basis Function

Since radial basis functions cannot be used in direct estimation, in this study, the estimation approach with conditioned radial basis functions, which is suitable for resource estimation, that guarantees positive definiteness and where the estimation results are within the desired limits, is used. This approach differs from the original approach in two points:

- 1) In estimation, only neighboring data is used.
- 2) Changing the kernel function cr parameter if the estimation is not within the desired range.

The goal in the first step given above is to increase the probability that the results to be in the desired range by performing regional conditioning. However, the results obtained in this step may not always be within the desired ranges. For this reason, an additional step was needed in the method. In this step, if the estimation is not within the desired range, the cr parameter shown in Table 1 is changed systematically. cr value is assigned, starting from zero, and it is checked whether the estimated value is within the desired range. The cr value is increased until the estimation is within the desired range.

2. Case Study

A coal field in the Türkiye-Thrace region was used for the application. A total of 128 vertical drillings with a length of 38 326 m were made in the field. The total thickness of coal cut from these drillings is 876 m. The coal seams are relatively thin, and the thickness of the coal seam is 6.5 m. The drillings made are shown in Figure 1.

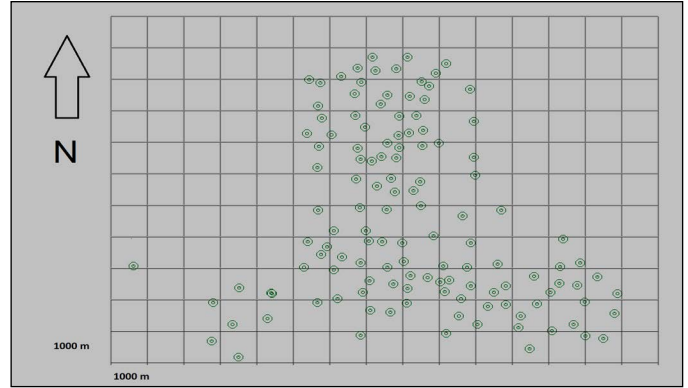


Figure 1. Plan view of the drillings

As seen in Figure 1, the average distance between the drillings is 500 m and the drilling frequency varies. Drilling frequency is approximately 800 m in the southwestern parts, while it is around 400 m in the northern parts. For the purpose of estimation, first of all, a 3D geological model of the coal seam was created. The section method, which is the most commonly used method in creating a geological model, was used and the model obtained is shown in Figure 2.

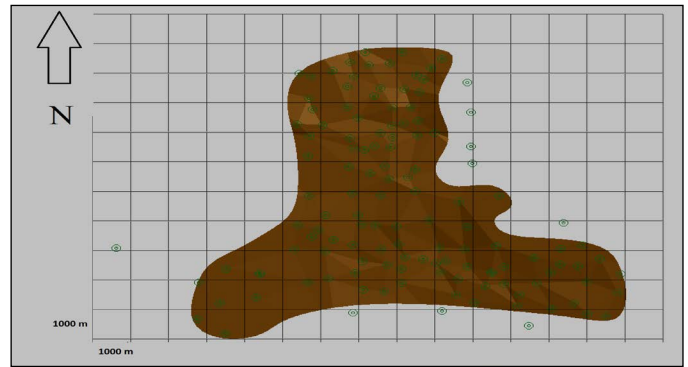


Figure 2. Solid model top view

With the creation of the 3D solid model, a block model was created to make estimations. Block dimensions were determined as 25 x 25 and 1 m in X, Y and Z directions, respectively. As a result of this process, the total blocks were created, and these are shown in Figure 3.

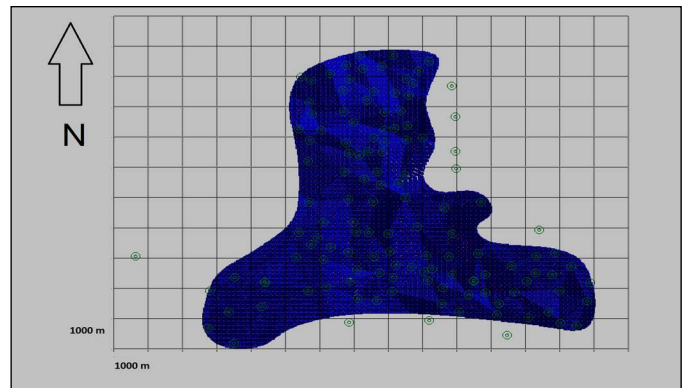


Figure 3. Block model top view

Data were composited at 1 m length for estimation with kriging and conditioned radial basis function. Summary statistics of the obtained data are shown in Table 2. Since the average distance between the data varies considerably, calculating the mean of the data directly may lead to erroneous inferences (Stein,2012, Tercan 2004). For this reason, declustered means of the data were calculated while calculating the declustered average, the existing area was divided into 1000 m x 1000 m intervals, and the data falling within these intervals was redefined according to the number of data whose weights fell on the average.

Table 2. Summary statistics of the composites

Number of data	Minimum	Average	Declustered Mean	Median	Maximum	Standard deviation
270	41	1428	1544	1456	3116	483

As can be seen in Table 2, the mean value and the declustered mean value are relatively different from each other. This is because the average distance between the data differs significantly. In this case, the mean for declustered data is higher than raw data. This means more frequent drilling in areas with low calorific value is made.

2.1 Estimation with Kriging

For estimation by kriging, firstly, the experimental variogram was calculated. Data frequency and spread did not allow for the computation of consistent directional variograms. For this reason, the experimental variogram was calculated and fitted as isotropic in the horizontal direction. The fitted variogram model is given in Table 3.

Table 3. Fitted variogram model

C_0	C	a (Horizontal, m)	a (Vertical, m)
83 000	150 000	1100	4

The cross-validation method was used to determine the usability of the adapted variogram in estimations. Cross validation results are shown in Table 4.

Table 4. Cross validation results

Mean	-10.23
Variance	255060
Average kriging variance	238269
Percentage of errors within two std. deviation	94.56

While the mean error was determined as low as -10 kCal/kg, the variance and mean kriging variances were close to each other. Also, Percentage of errors within two standard deviations, was a high value of 94.56%. Taking all these conditions into account, the cross-validation results show the usability of the variogram model for predictions. Estimation was performed using the fitted variogram model and summary statistics on the estimation results obtained Table 5 and the estimation map is given in Figure 4.

Table 5. Summary statistics of kriging estimate

Minimum (kCal/kg)	518
Median (kCal/kg)	1506
Average (kCal/kg)	1499
Maximum (kCal/kg)	2350
Standard deviation	134.57

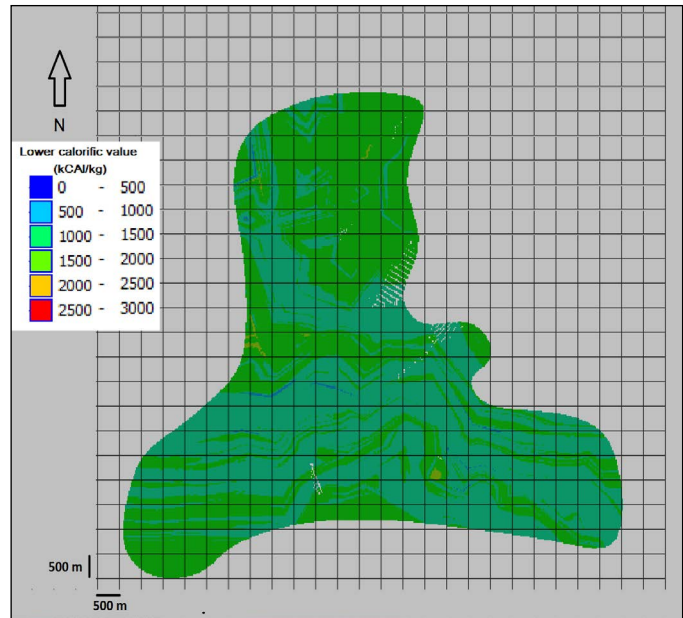


Figure 4. Kriging estimate of roof of the coal model

As can be seen in Table 5, the estimations using kriging were found between 518 and 2350 kCal/kg with an average of 1499 kCal/kg. In addition, in Figure 4, consistent with the calorific value summary statistics, the coal ceiling is with relatively low variability in the range of 1000 to 2000 kCal/kg.

2.2 Estimation with Conditioned Radial Basis Function (CRBF)

Estimation with the conditioned radial basis function is made using the steps described in the relevant section. The same block model and composites were used as in kriging. There is currently no program for estimation with conditioned radial basis functions. For this reason, the algorithm was written in MATLAB environment and a program that made predictions was written.

As seen in Table 6, there is more than one alternative that can be used as a kernel function in a radial basis function. It is necessary to determine which of these alternatives is to be used. After determining the kernel function to be used, parameter optimization of the relevant kernel function should be done. In the optimization of the kernel function and parameter, many alternatives have been tried and the option that produces the average closest to the average of the composites from these alternatives has been preferred. The estimation range was between 40 and 3000 kCal/kg, considering the lowest and highest values of the composite values. As a result, estimation was performed using the MATLAB code written to perform the estimation. Gaussian kernel function distribution parameter is preferred as 1.9 in estimation. The statistics of the obtained results are given in Table 6 and the estimation map is shown in Figure 5.

Table 6. Summary statistics of CRBF estimate

Minimum (kCal/kg)	40
Median (kCal/kg)	1570
Average (kCal/kg)	1542
Maximum (kCal/kg)	3001
Standard deviation	500.47

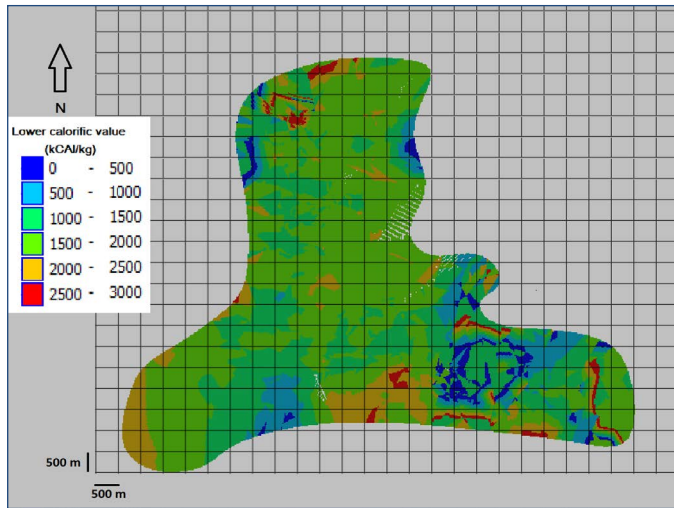


Figure 5. CRBF estimate of roof of the coal model

In Table 6, coal is estimated between 40 and 3001 kCal/kg with an average of 1542 kCal/kg. In addition, the standard deviation of the estimation is 500.47. Coal quality variability is relatively higher, and high-quality coal and low-quality coal are adjacent to each other in the south of the field.

In order to compare estimation results, histograms of the composites and estimation results are given in Figure 6.

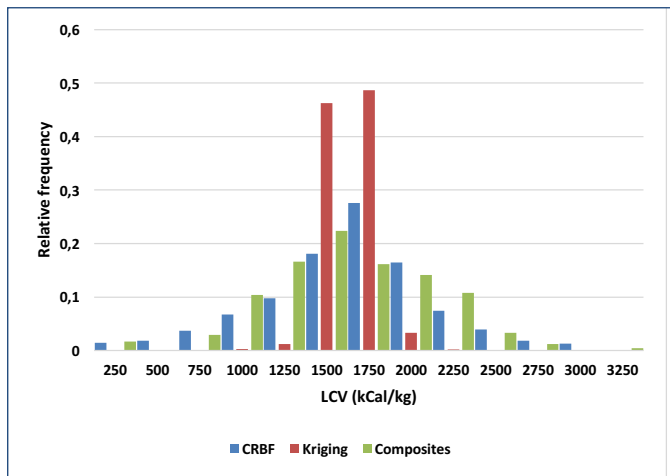


Figure 6. Histograms of CRBF, kriging and composites

As seen from the Figure 6 kriging estimates are centered between 1500 and 2000 kCal/kg values while it is expected due to the well-known smoothing property of the method. CRBF estimates are close to composite values while deviation exists at calorific values between 2250 and 2750 kCal/kg. To compare summary statistics of the estimate's percent of deviations from composite

statistics are given in Table 7 while percentages of deviations are calculated as in Eq. 8.

$$Deviation (\%) = \frac{(Stat.of\ estimates.-Stat\ of\ composites)}{Stat.of\ composites} * 100 \quad (8)$$

Table 7. Deviation of summary statistics of estimates from composite summary statistics

Deviation	CRBF	Kriging
Minimum (%)	-2.44	1163.41
Median (%)	4.28	1.37
Average (%)	7.83	3.43
Maximum (%)	-3.74	-24.60
Standard deviation(%)	3.50	-72.17

As seen from Table 7 deviation of the CRBF estimates are lower in minimum, maximum and standard deviation while kriging estimates produced closer estimates to composites in terms of median and average. The deviation of the kriging is dramatic in minimum and standard deviation which is result of smoothing.

3. Results and Discussions

In this study, Conditioned Radial Basis Function, and kriging methods for spatial estimation of quality are used and compared. For the purpose of comparison, a coal field in the Türkiye-Thrace region has been used. The spatial distribution of the coal calorific value was estimated by both methods. Experimental variograms were calculated and modeled for estimation by kriging. The experimental variogram shows that the average calorific value continuity in the field is approximately 1100 m and 4 m in horizontal and vertical directions respectively. Estimates are also made with the CRBF for comparison purposes. The Gaussian kernel function was used, and the cr was determined as 1.9.

It was observed that the average of the CRBF estimates were closer to composite estimates. In addition, the estimation interval of the CRBF is closer to the raw data. From this point of view, it has been observed that CRBF produces more desirable results in terms of estimation. However, the minimum value obtained with CRBF is 1 kCal/kg lower than the composite minimum values. Although this value may seem insignificant, it may indicate one of the flaws of estimation with CRBF. Because, in general, estimators are expected to interpolate, but as it can be seen, CRBF estimated a value outside the range of composites, albeit at an insignificant level. The highest estimate values obtained by both methods were lower than the composite estimates.

Estimation steps with both methods are similar while only attachment of the weights associated with the sampling points are only the difference. In estimation with kriging variogram values were used while in CRBF kernel function used instead. No variogram modelling is required in estimation with CRBF instead estimation of cr value is required. Results show that CRBF can be used as an alternative to kriging while technique can be used to check the estimations with kriging.

The parameters used in the method were determined by trial-and-error method. This approach is troublesome and the kernel function to be used may differ depending on the person using the method. Similarly, the parameters of the kernel function were determined by trial-and-error method. For this reason, it is necessary to develop standard methods for the determination of the kernel function and its related parameter. The method has been tried for the first time in the coal field. Testing the method with

other coal quality variables is important in terms of testing the usability of the method.

References

- Afzal P. (2018) Comparing ordinary kriging and advanced inverse distance squared methods based on estimating coal deposits; case study: East-Parvadeh deposit, central Iran. *J Min Environ* 9:753–760
- Atalay F, Tercan A.E. (2017) Coal resource estimation using Gaussian copula. *Int J Coal Geol* 175:1–9
- Atalay, F., Ünal, M. S., & Killoğlu, S. Y. (2021). Comparison of Radial Basis Function and Ordinary Kriging Estimations in an Iron Ore Deposit. *Avrupa Bilim ve Teknoloji Dergisi*, (27), 303-310 (In Turkish). <http://doi.org/10.1016/j.coal.2017.03.010>
- Cressie N. (1990) The origins of kriging. *Math Geol* 22:239–252
- Chelgani, S. C. (2021). Estimation of gross calorific value based on coal analysis using an explainable artificial intelligence. *Machine Learning with Applications*, 6, 100116. DOI: doi.org/10.1016/j.mlwa.2021.100116
- Demirel I.H., Sarac C., Sen O. (2000) Geostatistical reserve estimation: A case study in the Canakci coal seam of Ermenek Basin, Turkey. *Energy sources* 22:925–933
- Ertunc G., Tercan A.E., Hindistan M. A., Ünver, B., Ünal S., Atalay F., Killoğlu S.Y., (2013) Geostatistical estimation of coal quality variables by using covariance matching constrained kriging. *Int J Coal Geol* 112:14–25. <https://doi.org/10.1016/j.coal.2012.11.014>
- Fang J.H., Starks T.H., Mattern J. (1980) Geostatistical Approach in Coal Resource Estimation. *AAPG Bulletin* 64:705
- Hardy R. L. (1971), Multiquadratic equations of topography and other irregular surfaces, *J. Geophys. Res.*, 76, pp. 1905-1915
- Inaner H., Nakoman E., Karayigit A.I. (2008), Coal resource estimation in the Bayir field, Yatagan-Mugla, SW Turkey. *Energy Sources, Part A* 30:1005–1015
- Jeuken R., Xu C., Dowd P. (2020) Improving Coal Quality Estimations with Geostatistics and Geophysical Logs. *Nat Resour Res* 1–18 <https://doi.org/10.1007/s11053-019-09609-y>
- Journel A.G., Huijbregts C.J. (1978) *Mining geostatistics*. Academic press London
- Myers D.E. (1992) Kriging, cokriging, radial basis functions and the role of positive definiteness. *Comput Math with Appl* 24:139–148
- Olea, R. A., Luppens, J. A., & Tewalt, S. J. (2011). Methodology for quantifying uncertainty in coal assessments with an application to a Texas lignite deposit. *International Journal of Coal Geology*, 85(1), 78-90. <https://doi.org/10.1016/j.coal.2010.10.001>
- Olea R.A. (2012) *Geostatistics for engineers and earth scientists*. Springer Science & Business Media
- Orr M.J.L., (1996), *Introduction to radial basis function networks*, Centre for cognitive sciences, University of Edinburgh,
- Pardo-Igúzquiza E., Dowd P.A., Baltuille J.M., Chica-Olmo M. (2013) Geostatistical modelling of a coal seam for resource risk assessment. *Int J coal Geol* 112:134–140
- Rossi M.E., Deutsch C. V. (2013) *Mineral resource estimation*. Springer Science & Business Media
- Rossi M.E., Deutsch C. V. (2014) *Spatial Variability in Mineral Resource Estimation*. Springer, pp 97–116
- Schaback, R., Wendland, H. (2001). Characterization and construction of radial basis functions. *Multivariate approximation and applications*, 1-24.
- Schagen, I. P. (1979). Interpolation in two dimensions—a new technique. *IMA Journal of Applied Mathematics*, 23(1), 53-59.
- Sideri D., Roumpos C., Pavloudakis F, et al (2020) Multivariate Geostatistical Modeling of Lower Calorific Value in Multi-Seam Coal Deposits. *Appl Sci* 10:6208 <https://doi.org/10.3390/app10186208>
- Srivastava R.M. (2013) *Geostatistics: a toolkit for data analysis, spatial prediction and risk management in the coal industry*. *Int J Coal Geol* 112:2–13
- Stein M.L. (2012) *Interpolation of spatial data: some theory for kriging*. Springer Science & Business Media
- Tercan A.E. (2004) Global recoverable reserve estimation by covariance matching constrained kriging. *Energy sources* 26:1177–1185
- Tercan A.E., Karayigit A.I. (2001) Estimation of lignite reserve in the Kalburcayiri field, Kangal basin, Sivas, Turkey. *Int J Coal Geol* 47:91–100
- Tercan A.E., Ünver B., Hindistan M.A., (2013) Seam modeling and resource estimation in the coalfields of western Anatolia. *Int J Coal Geol* 112:94–106
- Turkish Coal Enterprises, (2021) *Coal Sector Report*, 119 pages.
- Thomas L. (2013) *Coal geology*. Wiley Online Library
- Whateley, M. K. G., Inaner, H., Nakoman, E., & Mulcahy, S. (1997). Comparison of classical and geostatistical methods for coal resource estimation in the Turgut Deposits, Muğla-Yatağan, SW Turkey. In *European Coal Geology, Proceeding 3rd European Coal Conference* (pp. 559-572).

ISSN 2564-7024



9 772564 702003